

# Stress release model and proxy measures of earthquake size. Application to Italian seismogenic sources

Elisa Varini<sup>1</sup>, Renata Rotondi<sup>1</sup>, Roberto Basili<sup>2</sup>, and Salvatore Barba<sup>2</sup>

<sup>1</sup>Istituto di Matematica Applicata e Tecnologie Informatiche *Enrico Magenes*, Consiglio Nazionale delle Ricerche (CNR), Milan, Italy

<sup>2</sup>Istituto Nazionale di Geofisica e Vulcanologia (INGV), Rome, Italy

**Corresponding author:** Elisa Varini. Address: CNR-IMATI, via Bassini 15, 20133 Milan (Italy). E-mail: elisa@mi.imati.cnr.it

## Abstract

This study presents a series of self-correcting models that are obtained by integrating information about seismicity and fault sources in Italy. Four versions of the stress release model are analyzed, in which the evolution of the system over time is represented by the level of strain, moment, seismic energy, or energy scaled by the moment. We carry out the analysis on a regional basis by subdividing the study area into eight tectonically coherent regions. In each region, we reconstruct the seismic history and statistically evaluate the completeness of the resulting seismic catalog.

---

### Abbreviations:

SR	stress release
MR	macroregion
McMC	Markov chain Monte Carlo
ISS	Individual Seismogenic Sources
CSS	Composite Seismogenic Sources

19 Following the Bayesian paradigm, we apply Markov chain Monte Carlo methods  
20 to obtain parameter estimates and a measure of their uncertainty expressed by the  
21 simulated posterior distribution. The comparison of the four models through the  
22 Bayes factor and an information criterion provides evidence (to different degrees  
23 depending on the region) in favor of the stress release model based on the energy  
24 and the scaled energy. Therefore, among the quantities considered, this turns out  
25 to be the measure of the size of an earthquake to use in stress release models. At  
26 any instant, the time to the next event turns out to follow a Gompertz distribution,  
27 with a shape parameter that depends on time through the value of the conditional  
28 intensity at that instant. In light of this result, the issue of forecasting is tackled  
29 through both retrospective and prospective approaches. Retrospectively, the fore-  
30 casting procedure is carried out on the occurrence times of the events recorded in  
31 each region, to determine whether the stress release model reproduces the observa-  
32 tions used in the estimation procedure. Prospectively, the estimates of the time to  
33 the next event are compared with the dates of the earthquakes that occurred after  
34 the end of the learning catalog, in the 2003-2012 decade.

35 **Keywords.** Point process; Probabilistic forecasting; Interevent time distribution;  
36 Seismogenic sources; Bayesian inference.

## 37 1 Introduction

38 The formulation of stochastic models for seismic hazard assessment in probabilistic terms  
39 is essentially based on phenomenological analyses or physical hypotheses. Phenomenolog-  
40 ical analyses generate models that belong to the class of the self-exciting models (Hawkes  
41 & Oakes , 1974) that describe the temporal and spatial clustering of earthquakes (Kagan  
42 1991; Ogata 1988, 1999; and references therein). These models were originally proposed  
43 to explain the decay of secondary shocks that follow a strong earthquake, and then they  
44 were applied for the detection of anomalies in seismic activity (Matsu'ura 1986; Ogata  
45 1997). These empirical models aspire to provide a good descriptive fit to the data, but  
46 they do not necessarily strive for a context-specific physical explanation. Models based on

47 physical hypotheses are more challenging, as these embody features that relate directly  
48 to the underlying scientific knowledge. Using these models, the aim is to explain how  
49 the evolution of the process depends on its history, in ways that can be interpreted in  
50 terms of the underlying mechanisms. Examples of such physical models are the block-  
51 slider, the branching for fractures, percolation, and cellular automata (Bhattacharyya &  
52 Chakrabarti et al. , 2006); these operate typically on small space-time scales. The most  
53 popular models that attempt to incorporate physical conjecture into the probabilistic  
54 framework and are concerned with large space-time scales are those included in the class  
55 of self-correcting models. In the seismological context, the elastic rebound theory still  
56 has the leading role, even though it was proposed a century ago by Reid (Reid , 1910).  
57 As a first approximation, modern measurements using global positioning systems (GPS)  
58 largely support the Reid theory as the basis of seismic movement along faults. Vere-Jones  
59 (1978) transposed this Reid theory into the framework of stochastic point processes, and  
60 in particular of the self-correcting models, through the first version of the stress release  
61 model. Enriched versions of this model have been extensively adopted for over 20 years  
62 now (Vere-Jones & Yonglu 1988; Zheng & Vere-Jones 1991, 1994; Bebbington & Harte  
63 2003; Kuehn et al. 2008). One of their peculiarities is that they allow for possible inter-  
64 actions among neighboring fault segments as an explanation for the presence of clusters  
65 of even large earthquakes, in contrast to the quiescence that one would expect after a  
66 strong earthquake, according to the elastic rebound theory.

67 The stress release (hereinafter SR) model is based on a physical quantity that rep-  
68 represents a proxy measure of the size of an earthquake, and that is generically indicated  
69 as ‘stress’. Translating the ‘elastic rebound theory’ into stochastic terms, the occurrence  
70 probability in a SR model depends on the elastic stress stored on a fault, which is the  
71 result of its gradual accumulation due to tectonic forces, and of sudden releases during  
72 past earthquakes.

73 In this study, we focus on alternative choices for the proxy variable ‘stress’ to identify  
74 which physical quantity among those considered produces the best performance of the  
75 model. We propose four versions of the SR model in which the evolution of the system

76 over time is represented by the amount of strain, seismic moment, seismic energy, or  
77 scaled energy. The values of these quantities for the events considered are obtained by  
78 integrating the available information on the most common input to probabilistic seismic  
79 hazard assessment, that is, the historical (macroseismic) and instrumental catalogs of  
80 seismicity, which are characterized by epicentral/ hypocentral location, origin time, and  
81 magnitude, and the map of seismogenic faults, as active faults deemed to be sources of  
82 large earthquakes and characterized by rupture parameters, such as area, mechanism, and  
83 magnitude.

84 In the literature the SR model was initially applied to strong earthquakes located in  
85 wide tectonic units, such as the northern China region (Vere-Jones & Yonglu , 1988). Then  
86 it turned out that the model fit can be improved by subdividing the region on the basis  
87 of seismicity, geophysical structure, and tectonic features, and by applying a different SR  
88 model to each subregion (Zheng & Vere-Jones 1991, 1994). Analogously, in Section 2, the  
89 four versions of the SR model are analyzed on a regional basis, by subdividing the Italian  
90 territory into eight large tectonically coherent zones, hereinafter called the macroregions  
91 (MRs). Using publicly available databases (Section 3), we put together eight datasets,  
92 one for each MR, that are constituted by earthquakes of  $M_w \geq 5.3$  that are most likely  
93 associated with the fault sources that are included in each MR. Statistical treatment of the  
94 possible incompleteness of the recorded seismicity is also taken into account (Appendix  
95 A).

96 In Section 4, the model parameters are estimated following the Bayesian paradigm and  
97 applying Markov chain Monte Carlo (MCMC) methods for sampling from the posterior  
98 probability distributions of the parameters. In this way, we obtain not only the parameter  
99 estimates, typically as their posterior means, but also a measure of their uncertainty, as  
100 expressed through the simulated posterior distribution of each parameter. In Section 4.2,  
101 the four models are compared one to the other through the Bayes factor and the Ando &  
102 Tsay information criterion (Ando & Tsay , 2010), to determine which among the proposed  
103 measures of the size of an earthquake provides the best fit to the data, and which resulting  
104 model shows the best predictive accuracy. We have also examined the various models in

105 the light of the probability distribution  $F(\omega_t|\mathcal{H}_t)$  of the ‘time to next event’ conditioned  
106 on the previous history  $\mathcal{H}_t$  of the process. Results of the four SR models fitted to the  
107 data of each MR are shown in Section 5, and their performances are compared with each  
108 other and also with those of the Poisson model. Retrospective validation is performed by  
109 evaluation of the expected time to the next event immediately after each earthquake in  
110 the datasets (Section 5.2.2). The same analysis is then carried out in a prospective sense,  
111 which considers the earthquakes that occurred from the end of the learning catalog to the  
112 end of 2012 (Section 5.2.3). These test events were drawn from the available instrumental  
113 and parametric catalogs, while remaining as consistent as possible with the characteristics  
114 of the learning catalog.

115 All of the forecasts were carried out using data based on 2002 knowledge, as they were  
116 made available by the database compilers, so that our results are independent of subjective  
117 choices and only reflect the capability of the applied model in an actual context.

## 118 2 Self-correcting models

119 Let us take into account a region that can be considered as a seismic unit on the basis,  
120 for instance, of the kinematic context and the expected rupture mechanism, and with  
121 a sufficiently extensive historical record. Adopting the Reid elastic-rebound theory, we  
122 generically use the word ‘stress’ to indicate the quantity  $X$  that governs the state of the  
123 system in that region. We assume that  $X$  increases linearly with time at a constant  
124 loading rate  $\rho$  imposed by external tectonic forces, until it exceeds the strength of the  
125 medium.  $X$  then abruptly decreases each time an earthquake occurs. This hypothesis  
126 can be formalized by:

$$127 \quad X(t) = X_0 + \rho t - S(t), \quad (1)$$

128 which expresses the variation of  $X(t)$  over  $t \in [0, T]$ , where  $X_0$  is the initial level of ‘stress’  
129 and  $S(t)$  is the accumulated ‘stress’ released by the earthquakes in the region at times  
130  $0 < t_i < t$ , which is  $S(t) = \sum_{i:t_i < t} X_i$ . Assuming that the probability  $\lambda(t)$  of instantaneous  
131 occurrence in  $(t, t + dt)$  is a monotonic increasing function  $\psi$  of the ‘stress’ level, we have

132  $\lambda(t|\mathcal{H}_t) = \psi[X(t)]$  where  $\mathcal{H}_t$  is the accumulated history of the process. In the original  
 133 version of this model, given by Vere-Jones (1978), the form of the intensity function  
 134 was  $\lambda(t) = [\nu + \beta(t - \tau S(t))]^+$ , where  $[x]^+$  is 0 if  $x < 0$ ; otherwise  $[x]^+ = x$ . Then, to  
 135 guarantee the positivity of  $\lambda$ , an exponential function for  $\psi$  was chosen such that:

$$136 \quad \lambda(t|\mathcal{H}_t) = \exp\{\nu + \beta X(t)\} = \exp\{\nu + \beta[X_0 + \rho t - S(t)]\} \quad (2)$$

137 with  $\beta > 0$ .

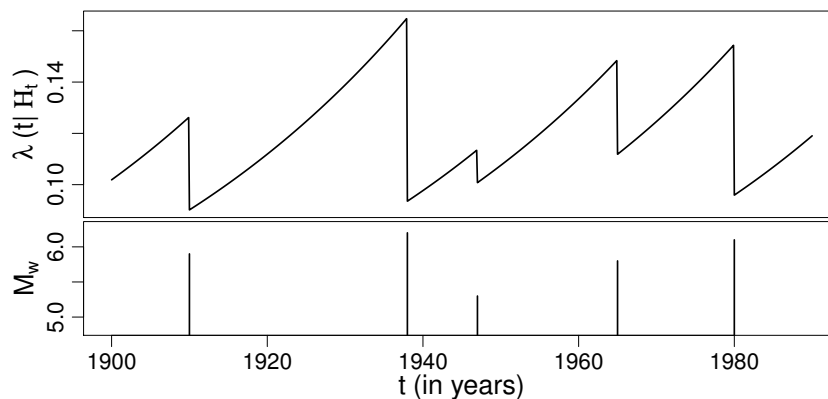


Figure 1: Representation of the conditional intensity function  $\lambda(t|\mathcal{H}_t)$  of the stress release model (top); moment magnitude versus occurrence times of the related seismic dataset (bottom).

138 This implies that when  $X(t)$  assumes a positive and larger value (i.e., low seismic  
 139 activity), the intensity  $\psi[X(t)]$  is also larger, and the occurrence probability increases;  
 140 conversely, smaller negative values of  $X(t)$  reduce the probability (Figure 1). This model  
 141 belongs to the class of self-correcting point processes of Isham & Westcott (1979), with  
 142 history-conditioned intensities. In other words, the model given by Equation (2) can  
 143 be thought of in terms of the balance between the expected and observed values of the  
 144 physical quantity  $X$ . In Equation (1), at each  $t_i$ , it can be seen that  $X_0 + \rho t_i$  is the  
 145 estimated ‘stress’ in the region, whereas  $S(t_i)$  is the stress released by all of the earthquakes  
 146 before  $t_i$ , and thus represents the lowest boundary of the stress estimate in the region.  
 147 This line of reasoning implies that when the observed accumulated stress is lower than  
 148 the expected, a seismic event is more likely to occur.

149 In Equation (2),  $X$  can be any physical parameter that constitutes a proxy measure  
150 of the strength of an earthquake, with the only constraint being that when dealing with  
151 long-term seismic hazard, this physical quantity can be evaluated from historical events.  
152 In the first applications of the stochastic model given by Equation (2) (Vere-Jones &  
153 Yonglu 1988; Zheng & Vere-Jones 1991, 1994),  $X(t)$  is a scalar quantity - the Benioff  
154 strain - that can be calculated from:

$$155 \log_{10} X = \frac{1}{2} \log_{10} E = 0.75 M_s + 2.4 \quad (3)$$

156 where  $E$  is the unknown seismic energy and  $M_s$  is the earthquake magnitude, which  
157 incorporates proportionality between the stress drop and the square root of the energy  
158 release (Benioff, 1951). To also take into account the contribution of energy lost to heat  
159 during an earthquake, the seismic moment  $M_0$ , given by:

$$160 \log_{10} M_0 = 1.5 M_w + 9.1 \quad (M_0 \text{ in } Nm), \quad (4)$$

161 (Kanamori & Brodsky, 2004) better represents the total seismic release. Note that  $M_s$   
162 and  $M_w$  do not differ significantly for earthquakes with rupture lengths of 100 km or less  
163 (Kanamori, 1977).

164 The seismic moment depends on the coseismic displacement, and it is a static measure  
165 of the earthquake size related to its long-term tectonic effects. In contrast, the radiated  
166 energy is a dynamic measure of seismic potential for damage to anthropogenic structures.  
167 Hence energy and moment can be considered as complementary size measures in the esti-  
168 mation of seismic hazard. For recent earthquakes, however, the seismic energy computed  
169 through direct spectral analysis of broadband seismic waveforms can have significant re-  
170 gional and tectonic variations (Choy & Boatwright, 1995) that are largely neglected  
171 when using empirical formulae. In the case of historical earthquakes, ways to measure  
172 the amount of energy released that contain information on source, tectonic setting, and  
173 faulting mechanism can compensate for the inability to provide direct measurements of  
174 the energy.

175 Several studies have analyzed the scaling relationship for the apparent stress as a  
176 function of the seismic moment  $M_0$ , the rupture area  $A$ , and the average slip acceleration  
177 (Senatorski 2005, 2006). Considering different earthquake sets, from mining-induced,  
178 to small-to-moderate, and up to large earthquakes (Kanamori et al. , 1993), Senatorski  
179 (2007) deduced that the  $E$ - $M_0$  relationship is not linear, and the scatter in the log  $E$ -  
180 log  $M_0$  plot can be noticeably reduced by taking into account the rupture area. Hence he  
181 proposed the relationship:

$$182 \quad E \propto \frac{M_0^{1.5}}{\sqrt{A}}, \quad (5)$$

183 where  $A$  is the area of the fault surface that ruptures during an earthquake. Rupture area  
184  $A$  is hereafter approximated by using the well-known regressions of Wells and Coppersmith  
185 (1994; see Section 4.1 for more details). Another influential seismic parameter that gives  
186 information on the rupture behavior (Kanamori & Heaton , 2000) is the scaled energy  $E_s$ ,  
187 a non-dimensional radiated energy scaled with  $M_0$ , such that:

$$188 \quad E_s = \frac{E}{M_0}. \quad (6)$$

189 Substituting the expression of Equation (5) for  $E$  in Equation (6), the following expression  
190 for the scaled energy is obtained:

$$191 \quad E_s \propto \frac{M_0^{0.5}}{\sqrt{A}}. \quad (7)$$

192 In the present study, we examine the four different versions of the SR model (Eq.  
193 2) that can be obtained by substituting  $X$  with the Benioff strain  $X_B$  (3), the seismic  
194 moment  $X_M$  (4), the seismic energy  $X_E$  (5), or the scaled energy  $X_S$  (7). The four models



195 depend on the magnitude and threshold magnitude  $M_{th}$ , and are expressed by:

$$196 \quad X_B = 10^{0.75 (M_w - M_{th})}, \quad (8)$$

$$197 \quad X_M = 10^{1.5 (M_w - M_{th})}, \quad (9)$$

$$198 \quad X_E = \frac{10^{2.25 (M_w - M_{th})}}{\sqrt{A}}, \quad (10)$$

$$199 \quad X_S = \frac{10^{0.75 (M_w - M_{th})}}{\sqrt{A}}, \quad (11)$$

200 Hereinafter, we denote these models as  $\mathbf{R}_B$ ,  $\mathbf{R}_M$ ,  $\mathbf{R}_E$ , and  $\mathbf{R}_S$ , respectively.

## 201 3 Databases

202 In the present study, we used two independently developed and publicly available databases  
203 (at the time this study was carried out): the Database of Individual Seismogenic Sources  
204 (DISS, version 3.0.2; DISS Working Group 2007), and the Parametric Catalog of Italian  
205 Earthquakes, version 2004 (CPTI04; CPTI Working Group 2004). These two databases  
206 reflect the level of knowledge at the end of 2002. To test our results we then used  
207 the most recent version of the Parametric Catalog of Italian Earthquakes, version 2011  
208 (CPTI11; Rovida et al. 2011), which extends the records to 2006, and from 2007 on-  
209 wards, we used the Italian Seismic Instrumental and parametric Data-base (ISIDe 2010;  
210 <http://iside.rm.ingv.it/iside/standard/index.jsp>).

### 211 3.1 Fault sources

212 DISS is a large repository of geological, tectonic and active fault data for Italy and the  
213 surrounding areas, which was compiled from first-hand experience of the authors and  
214 from a large amount of literature data (Basili et al. 2008; Basili et al. 2009). The  
215 database stores two main categories of parameterized crustal fault sources: Individual  
216 Seismogenic Sources (ISS) and Composite Seismogenic Sources (CSS), both of which are  
217 considered to be capable of releasing earthquakes of  $M_w$  5.5 or greater. In most cases, the  
218 ISS represent the preferred source solutions of well-known large earthquakes of the past

219 that ideally ruptured the fault from end to end (i.e., a fault segment). In recognition of  
220 the inherent difficulties in the identification of all possible fault segments in the tectonic  
221 record, however, in 2005 the DISS was extended to include the CSS, a source category  
222 that was also meant to expand the territorial coverage and completeness, and hence the  
223 capabilities, of the database. A CSS is essentially an active structure where the definition  
224 is based on regional surface and subsurface geological data that are exploited to identify  
225 and map entire fault systems. As opposed to the ISS, the termination of a CSS can be  
226 either an identified fault limit or a significant structural change. This implies that such  
227 fault sources can comprise an unspecified number of different potential ruptures, and can  
228 produce earthquakes of any size, at least in principle, up to an assigned maximum. The  
229 DISS (version 3.0.2) contains 81 such fault sources, most of which are located in Italy,  
230 whereas seven fault sources, which are not used in this study, are located in neighboring  
231 countries (Figure 2).

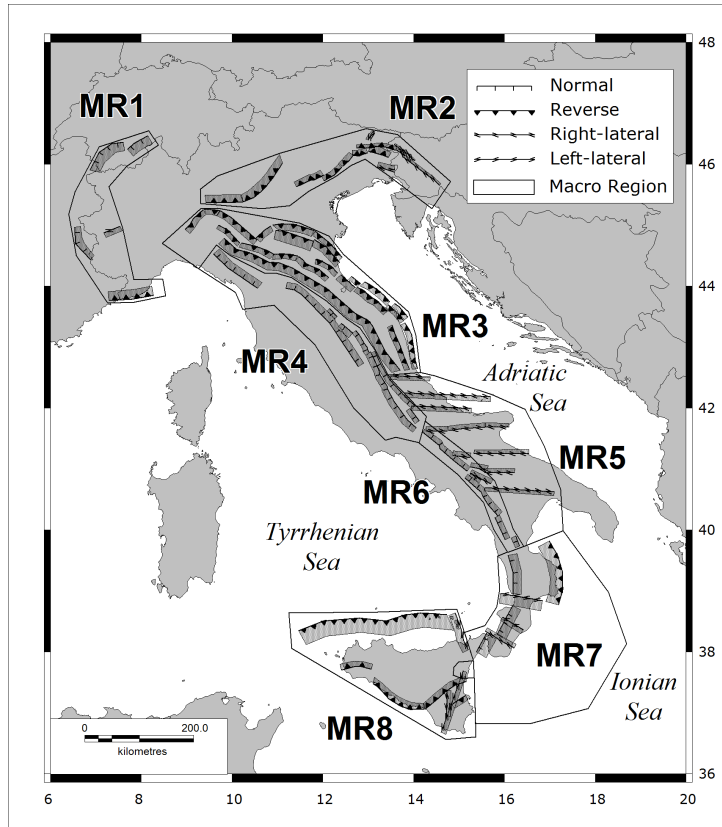


Figure 2: Map of the Composite Seismogenic Sources (CSS) from the DISS database, version 3.0.2 (DISS Working Group, 2007), classified according to the faulting mechanism. Shaded area: vertical projection of the fault plane to the ground surface. The outlined polygons are the MRs described in the text and Table 3.

## 232 3.2 Earthquakes

233 CPTI04 is a parametric catalog of earthquakes that exploits all of the sources of infor-  
 234 mation that are available in historical documents and published scientific studies. The  
 235 thresholds for including an earthquake in the catalog are as follows: for the pre-1980 sec-  
 236 tion, macroseismic intensity  $I_0 = V-VI$ , evaluated through the Mercalli-Cancani-Sieberg  
 237 scale (MCS), or  $M_s = 4.0$ ; for the post-1980 section,  $M_s = 4.15$ ; and for earthquakes  
 238 located in the Etna volcano area,  $M_s = 3.0$  (Figure 3).

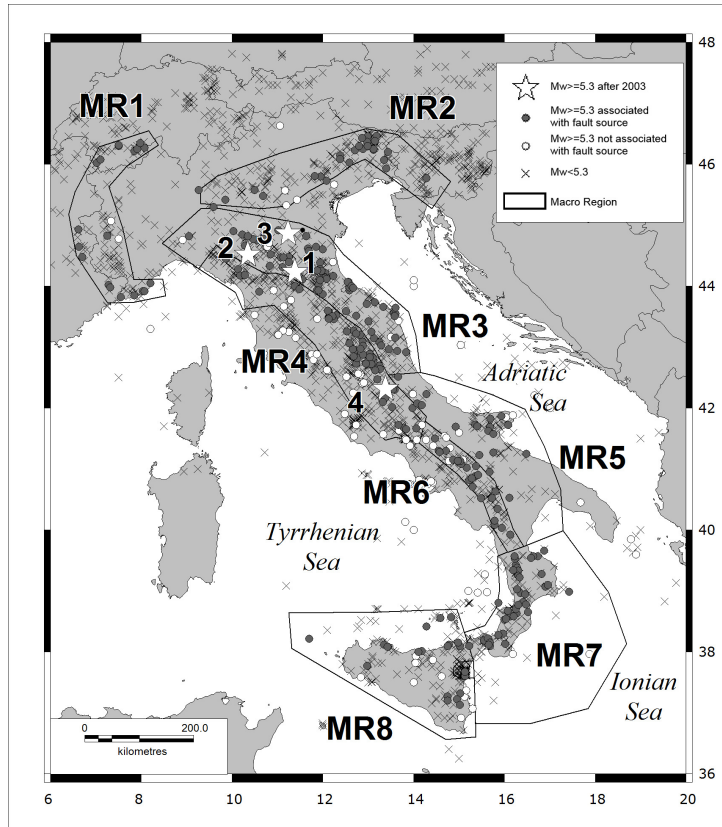


Figure 3: Map of earthquakes from the CPTI04 catalog (CPTI Working Group , 2004). The associations among the earthquakes, macroregions (MRs), and fault sources are listed in Tables 1-2. Stars indicate earthquakes that occurred after the end of the learning catalog, and were thus used to validate the forecast (see Section 5.2.3).

239 The catalog is supplied by the compilers in declustered form, such that the few his-  
 240 torical events that were recorded within 90 days and 30 km from the principal events  
 241 (mainshocks) in seismic sequences are not included. Each event in the catalog is charac-  
 242 terized by its origin time, location, number of macroseismic intensity points, maximum  
 243 and epicentral intensities, and moment and surface-wave magnitudes, which are based on  
 244 empirical relationships for older events and on instrumental catalogs for modern events.  
 245 ISIDE is a parametric catalog of seismicity that includes revised quasi-real-time earth-  
 246 quake locations based on data collected from the Italian National Seismic Network. The  
 247 sizes of the events are given in the local magnitude scale ( $M_l$ ). This catalog has been  
 248 published twice a month since April 16, 2005.

region	CSS	fault type	date	$M_w$	region	CSS	fault type	date	$M_w$	region	CSS	fault type	date	$M_w$									
MR <sub>1</sub>	22	R	1644/02/15	5.88				1971/07/15	5.61				1791/01/00	5.37									
			1818/02/23	5.55				1967/12/30	5.36				1815/09/03	5.37									
MR <sub>2</sub>	23	RL	1819/01/08	5.34				1828/10/09	5.67				1859/08/22	5.70									
			1831/05/26	5.54				1908/11/16	5.37				1873/07/12	5.40									
			1854/12/29	5.77				1943/10/03	5.81				1874/12/06	5.47									
			1887/02/23	6.29				1768/10/19	5.84				1904/02/24	5.67									
			1808/04/02	5.67				1781/06/03	6.23				1915/01/13	6.99									
			1802/05/12	5.67				1799/07/28	5.93				1916/11/16	5.48									
			1836/06/12	5.48				1869/06/25	5.32				1922/12/29	5.60									
	61	R	1901/10/30	5.67				1873/03/12	5.88				1964/08/02	5.44									
			1812/10/25	5.70				1873/09/17	5.52				1979/09/19	5.90									
			1873/06/29	6.33				1918/11/10	5.79				1984/05/07	5.93									
			1936/10/18	5.90				1937/12/10	5.42				1834/02/14	5.64									
			1776/07/10	5.82				1951/09/01	5.31				1837/04/11	5.65									
			1794/06/07	5.55				1972/11/26	5.34				1914/10/27	5.79									
			1920/05/05	5.48				1998/03/26	5.33				1920/09/07	6.48									
			1977/09/16	5.54				1916/05/17	5.85				1747/04/17	5.93									
			1931/12/25	5.36				1916/08/16	5.92				1751/07/27	6.30									
			1976/05/06	6.43				1972/06/14	5.40				1791/10/11	5.32									
	66	R	1976/09/15	5.92				1897/09/21	5.50				1838/02/14	5.63									
			1788/10/20	5.71				1924/01/02	5.59				1997/09/26	6.05									
			1908/07/10	5.34				1930/10/30	5.94				1745/03/00	5.37									
			1924/12/12	5.53				1786/12/25	5.67				1767/06/05	5.44									
			1928/03/27	5.75				1875/03/17	5.74				1789/09/30	5.80									
			1781/04/04	5.84				1786/04/07	5.31				1832/01/13	5.80									
			1781/07/17	5.53				1818/12/09	5.57				1854/02/12	5.37									
			1813/09/21	5.32				1929/04/20	5.55				1878/09/15	5.55									
			1870/10/30	5.59				1996/10/15	5.44				1910/06/29	5.37									
			1911/02/19	5.38				1796/10/22	5.63				1917/04/26	5.80									
	67	LL	1935/06/05	5.34				1909/01/13	5.53				1919/06/29	6.18									
			1963/08/09	5.32				1703/01/14	6.81				1762/10/06	5.90									
			1917/11/05	5.36				1703/02/02	6.65				2001/11/26	5.37									
			1831/09/11	5.48				1719/06/27	5.32				1984/04/29	5.68									
			1832/03/13	5.59				1730/05/12	5.85														
				1				R	1971/07/15				5.61				1971/07/15	5.61				1791/01/00	5.37
									1967/12/30				5.36				1967/12/30	5.36				1815/09/03	5.37
									1828/10/09				5.67				1828/10/09	5.67				1859/08/22	5.70
									1908/11/16				5.37				1908/11/16	5.37				1873/07/12	5.40
									1943/10/03				5.81				1943/10/03	5.81				1874/12/06	5.47
1768/10/19	5.84	1768/10/19			5.84	1904/02/24	5.67																
1781/06/03	6.23	1781/06/03			6.23	1915/01/13	6.99																
1799/07/28	5.93	1799/07/28			5.93	1916/11/16	5.48																
1869/06/25	5.32	1869/06/25			5.32	1922/12/29	5.60																
1873/03/12	5.88	1873/03/12			5.88	1964/08/02	5.44																
1873/09/17	5.52	1873/09/17	5.52	1979/09/19	5.90																		
	26	N	1918/11/10	5.79				1918/11/10	5.79				1984/05/07	5.93									
			1937/12/10	5.42				1937/12/10	5.42				1834/02/14	5.64									
			1951/09/01	5.31				1951/09/01	5.31				1837/04/11	5.65									
			1972/11/26	5.34				1972/11/26	5.34				1914/10/27	5.79									
			1998/03/26	5.33				1998/03/26	5.33				1920/09/07	6.48									
			1916/05/17	5.85				1916/05/17	5.85				1747/04/17	5.93									
			1916/08/16	5.92				1916/08/16	5.92				1751/07/27	6.30									
			1972/06/14	5.40				1972/06/14	5.40				1791/10/11	5.32									
			1897/09/21	5.50				1897/09/21	5.50				1838/02/14	5.63									
			1924/01/02	5.59				1924/01/02	5.59				1997/09/26	6.05									
1930/10/30	5.94	1930/10/30	5.94	1745/03/00	5.37																		
	37	N	1786/12/25	5.67				1786/12/25	5.67				1767/06/05	5.44									
			1875/03/17	5.74				1875/03/17	5.74				1789/09/30	5.80									
			1786/04/07	5.31				1786/04/07	5.31				1832/01/13	5.80									
			1818/12/09	5.57				1818/12/09	5.57				1854/02/12	5.37									
			1929/04/20	5.55				1929/04/20	5.55				1878/09/15	5.55									
			1996/10/15	5.44				1996/10/15	5.44				1910/06/29	5.37									
			1796/10/22	5.63				1796/10/22	5.63				1917/04/26	5.80									
			1909/01/13	5.53				1909/01/13	5.53				1919/06/29	6.18									
			1703/01/14	6.81				1703/01/14	6.81				1762/10/06	5.90									
			1703/02/02	6.65				1703/02/02	6.65				2001/11/26	5.37									
1719/06/27	5.32	1719/06/27	5.32	1984/04/29	5.68																		
	28	N	1730/05/12	5.85				1730/05/12	5.85														
			1971/07/15	5.61				1971/07/15	5.61														
			1967/12/30	5.36				1967/12/30	5.36														
			1828/10/09	5.67				1828/10/09	5.67														
			1908/11/16	5.37				1908/11/16	5.37														
			1943/10/03	5.81				1943/10/03	5.81														
			1768/10/19	5.84				1768/10/19	5.84														
			1781/06/03	6.23				1781/06/03	6.23														
			1799/07/28	5.93				1799/07/28	5.93														
			1869/06/25	5.32				1869/06/25	5.32														
1873/03/12	5.88	1873/03/12	5.88																				
	30	R	1873/09/17	5.52				1873/09/17	5.52														
			1918/11/10	5.79				1918/11/10	5.79														
			1937/12/10	5.42				1937/12/10	5.42														
			1951/09/01	5.31				1951/09/01	5.31														
			1972/11/26	5.34				1972/11/26	5.34														
			1998/03/26	5.33				1998/03/26	5.33														
			1916/05/17	5.85				1916/05/17	5.85														
			1916/08/16	5.92				1916/08/16	5.92														
			1972/06/14	5.40				1972/06/14	5.40														
			1897/09/21	5.50				1897/09/21	5.50														
1924/01/02	5.59	1924/01/02	5.59																				
	31	R	1930/10/30	5.94				1930/10/30	5.94														
			1786/12/25	5.67				1786/12/25	5.67														
			1875/03/17	5.74				1875/03/17	5.74														
			1786/04/07	5.31				1786/04/07	5.31														
			1818/12/09	5.57				1818/12/09	5.57														
			1929/04/20	5.55				1929/04/20	5.55														
			1996/10/15	5.44				1996/10/15	5.44														
			1796/10/22	5.63				1796/10/22	5.63														
			1909/01/13	5.53				1909/01/13	5.53														
			1703/01/14	6.81				1703/01/14	6.81														
1703/02/02	6.65	1703/02/02	6.65																				
	32	R	1719/06/27	5.32				1719/06/27	5.32														
			1730/05/12	5.85				1730/05/12	5.85														
			1971/07/15	5.61				1971/07/15	5.61														
			1967/12/30	5.36				1967/12/30	5.36														
			1828/10/09	5.67				1828/10/09	5.67														
			1908/11/16	5.37				1908/11/16	5.37														
			1943/10/03	5.81				1943/10/03	5.81														
			1768/10/19	5.84				1768/10/19	5.84														
			1781/06/03	6.23				1781/06/03	6.23														
			1799/07/28	5.93				1799/07/28	5.93														
1869/06/25	5.32	1869/06/25	5.32																				
	39	R	1873/03/12	5.88				1873/03/12	5.88														
			1873/09/17	5.52				1873/09/17	5.52														
			1918/11/10	5.79				1918/11/10	5.79														
			1937/12/10	5.42				1937/12/10	5.42														
			1951/09/01	5.31				1951/09/01	5.31														
			1972/11/26	5.34				1972/11/26	5.34														
			1998/03/26	5.33				1998/03/26	5.33														
			1916/05/17	5.85				1916/05/17	5.85														
			1916/08/16	5.92				1916/08/16	5.92														
			1972/06/14	5.40				1972/06/14	5.40														
1897/09/21	5.50	1897/09/21	5.50																				
	44	R	1924/01/02	5.59				1924/01/02	5.59														
			1930/10/30	5.94				1930/10/30	5.94														
			1786/12/25	5.67				1786/12/25	5.67														
			1875/03/17	5.74				1875/03/17	5.74														
			1786/04/07	5.31				1786/04/07	5.31														
			1818/12/09	5.57				1818/12/09	5.57														
			1929/04/20	5.55				1929/04/20	5.55														
			1996/10/15	5.44				1996/10/15	5.44														
			1796/10/22	5.63				1796/10/22	5.63														
			1909/01/13	5.53				1909/01/13	5.53														
1703/01/14	6.81	1703/01/14	6.81																				
	46	R	1703/02/02	6.65				1703/02/02	6.65														
			1719/06/27	5.32				1719/06/27	5.32														
			1730/05/12	5.85				1730/05/12	5.85														
			1971/07/15	5.61				1971/07/15	5.61														
			1967/12/30	5.36				1967/12/30	5.36														
			1828/10/09	5.67				1828/10/09	5.67														
			1908/11/16	5.37				1908/11/16	5.37														
			1943/10/03	5.81				1943/10/03	5.81														
			1768/10/19	5.84				1768/10/19	5.84														
			1781/06/03	6.23				1781/06/03	6.23														

region	CSS	fault type	date	$M_w$	region	CSS	fault type	date	$M_w$	region	CSS	fault type	date	$M_w$	
MR <sub>5</sub>	3	RL	1941/08/20	5.37				1998/09/09	5.68		68	LL	1783/03/01	5.92	
			2002/10/31	5.78				1694/09/08	6.87				1783/03/28	6.94	
	5	RL	1846/08/08	5.33		63	N	1910/06/07	5.87				1821/08/02	5.37	
			1990/05/05	5.84	MR <sub>7</sub>	15	N	1767/07/14	5.83					1905/09/08	7.06
	58	RL	1841/02/21	5.40					1835/10/12	5.91				1947/05/11	5.71
		1875/12/06	6.07				1854/02/12	6.15					2001/05/17	5.60	
		1889/12/08	5.55				1870/10/04	6.16			80	LL	1828/03/12	5.33	
		1893/08/10	5.44				1886/03/06	5.56		MR <sub>8</sub>	14	R	1613/08/25	5.57	
		1948/08/18	5.58				1887/12/03	5.52						1726/09/01	5.61
		1881/09/10	5.59				1913/06/28	5.65					1736/08/16	5.47	
	59	RL						1783/02/06	5.94				1739/05/10	5.54	
	75	RL	1950/09/05	5.73		16	N	1908/12/28	7.24				1823/03/05	5.87	
	79	RL	1933/09/26	5.68				1909/07/01	5.55				1892/03/16	5.38	
	84	N	1930/07/23	6.72				1975/01/16	5.38				1940/01/15	5.34	
	89	RL	1851/08/14	6.33				1824/12/11	5.53				1979/12/08	5.44	
MR <sub>6</sub>	24	N	1688/06/05	6.72		19	R	1832/03/08	6.48				1980/05/28	5.71	
			1702/03/14	6.32				1836/04/25	6.16				2002/09/06	5.89	
			1732/11/29	6.61				1917/06/12	5.50			17	LL	1693/01/11	7.41
			1805/07/26	6.57				1932/01/02	5.62					1818/02/20	6.00
			1905/11/26	5.32				1983/11/08	5.37					1914/05/08	5.30
			1962/08/21	6.19				1743/12/07	5.79					1968/01/15	6.12
		34	N	1826/02/01	5.68		53	N	1783/02/05	6.91				1624/10/03	5.57
			1853/04/09	5.90				1783/02/07	6.59					1818/03/01	5.63
			1857/12/16	6.96				1791/10/13	5.92					1717/04/22	5.40
			1980/11/23	6.89				1928/03/07	5.90					1786/03/10	6.02
	38	N	1708/01/26	5.61				1894/11/16	6.05				1926/08/17	5.32	
		1831/01/02	5.46			55	RL	1907/10/23	5.93				1978/04/15	6.06	
		1836/11/20	5.83												

Table 2: List of the earthquakes in MR<sub>5</sub>-MR<sub>8</sub> and their association to fault sources from DISS. Fault types: LL, left-lateral strike-slip; RL, right-lateral strike-slip; N, normal; R, reverse.

### 249 3.3 Dataset construction

250 To carry out the model analysis in a regionalized way, we subdivided the Italian territory  
 251 into eight large zones (see Table 3, Figures 2 and 3), which we refer to as the MRs (i.e.,  
 252 macroregions), because they are larger than the usual sizes of the zones in zonation models  
 253 that are used for standard seismic hazard assessments in Italy.

ID	Name	Mechanism
MR <sub>1</sub>	Western Alps	Mixed faulting mechanisms.
MR <sub>2</sub>	Eastern Alps	Dominating south-verging thrust faulting mechanism with some strike-slip faulting in the easternmost portion of the MR (Slovenia).
MR <sub>3</sub>	Central northern Apennines, east	Exclusively northeast-verging thrust faulting mechanism. Faulting depth is progressively shallower towards the northeast.
MR <sub>4</sub>	Central northern Apennines, west	Exclusively normal faults with NE-SW extension axis that affect the crest of the Apennine mountain chain.
MR <sub>5</sub>	Southern Apennines, Apulia	E-W trending right-lateral strike-slip faulting. Depth of faulting often deeper than in other regions.
MR <sub>6</sub>	Southern Apennines, west	Exclusively normal faults with NE-SW extension axis that affect the crest of the Apennine mountain chain.
MR <sub>7</sub>	Calabrian Arc	N-S to NE-SW trending normal faults, minor oblique-slip faults located inland, and thrust faults in the Ionian offshore. These last are mainly located in the overriding plate, and they are poorly mapped and difficult to associate with specific earthquakes.
MR <sub>8</sub>	Sicily	Dominating thrust faulting, north-verging in the Tyrrhenian offshore, south-verging inland. Strike-slip faulting in the southwestern corner of Sicily.

Table 3: Faulting mechanisms in the MRs.

254 To construct these MRs, we aggregated zones from the seismic ZS9 zonation (Meletti  
 255 et al. , 2008) based on their common tectonic characteristics, and refined the boundaries  
 256 to include fault sources that belong to the same tectonic domain. Earthquakes from  
 257 CPTI04 that are explicitly associated with an ISS based on geological/ geophysical studies  
 258 in the DISS are also associated with the CSS, which contains the ISS. The remaining

259 earthquakes are associated with the nearest CSS (Fracassi U. and Valensise G., personal  
 260 communication). Hence each dataset represents the activity of a system of faults which  
 261 belong to the same tectonic domain; this guarantees consistency with the assumptions  
 262 underlying the SR model and agreement with the case studies proposed in the literature.

263 To allow for potential underestimation of the earthquake magnitudes, we considered  
 264 all of the earthquakes with moment magnitude larger than 5.3. It is necessary to note  
 265 that the algorithm used for the locating of historical events from macroseismic data used  
 266 in CPTI04 cannot determine the hypocentral depth or reliably locate offshore events. The  
 267 latter are automatically located near the coast, and can be mistaken for actual coastal  
 268 events. To address the issue of the possible incompleteness of the catalog in the time span  
 269  $(T_0, T_f)$  covered by the data, we follow the statistical approach based on the detection  
 270 of a changepoint in the occurrence rate function (Rotondi & Garavaglia, 2002); this  
 271 point is meant as the beginning of the complete part of the catalog. The model and the  
 272 estimation procedure are briefly recalled in Appendix A. Table 4 summarizes the results  
 273 obtained for the eight MRs:  $\hat{h}_2$  and  $\check{s}$  are the estimates of the occurrence rates in the  
 274 complete part and of the changepoint. The method adopted tends to place the estimate  
 275  $\check{s}$  relatively close to  $t_1$  (the time of the first earthquake occurred after  $T_0$ ), where the  
 276 unknown stress level could be high. This means that the analysis of the phenomenon  
 277 started from a nonrandom point, but neglecting this piece of information. To overcome  
 278 this issue we moved  $\check{s}$  to  $T_c$ , so that the time interval that separates the beginning of the  
 279 complete part of the catalog from the first event is equal to the average interevent time,  
 280 which is calculated by also taking into account the censored observation related to the  
 281 time elapsed between the latest event and  $T_f$ . Thus, we have the relationship:

$$282 \quad T_c = t_1 - \frac{\sum_{i=1}^{n-1} (t_{i+1} - t_i) + (T_f - t_n)}{n - 1}. \quad (12)$$

283 Extending the analyzed time interval in this way, no events are added to the original  
 284 dataset. Thus, we start to observe the phenomenon when the stress level accumulated in  
 285 the system is reasonably small, and a recharge period is roughly at the beginning. Note  
 286 that the estimated changepoint of MR<sub>1</sub> falls beyond the most recent event (see 1887.15\*



287 in Table 4), which implies that the entire dataset can be considered as complete. Then,  
 288 by applying Equation (12) to the data after 1600, we have the year 1584 as the initial  
 289 time for the analysis.

290 Tables 1 and 2 list the earthquakes that make up the datasets analyzed below, which are  
 291 sorted according to MR and fault source.

region	$T_0$	$\check{s}$	$\hat{h}_2$	$T_c$
MR <sub>1</sub>	1448	1887.15*	0.0126	1584
MR <sub>2</sub>	1197	1776.52	0.0676	1762
MR <sub>3</sub>	1264	1781.25	0.164	1763
MR <sub>4</sub>	1244	1703.03	0.120	1695
MR <sub>5</sub>	1260	1841.13	0.0764	1829
MR <sub>6</sub>	985	1688.42	0.0461	1667
MR <sub>7</sub>	931	1767.53	0.108	1735
MR <sub>8</sub>	1168	1613.64	0.0488	1593

Table 4: Completeness of the learning datasets according to MR:  $\check{s}$  = posterior mode of the position of the changepoint,  $\hat{h}_2$  = posterior mean rate,  $T_c$  = left end of the time interval under examination (see Equation (12)), \* dataset considered as a complete set.

## 292 4 Bayesian inference and model comparison

293 A Bayesian approach to the analysis of the SR model is illustrated. Section 4.1 presents  
 294 the Bayesian method for parameter estimation of the four versions of the SR model  
 295 introduced in Section 2; then, Section 4.2 shows how these models can be tested through  
 296 global summary measures of model performance and earthquake forecast procedures.

### 297 4.1 Parameter estimation

298 In this section, we deal with the problems of estimating the model parameters, and then  
 299 of selecting the best model from the group of candidate models. Point processes are  
 300 characterized by their intensity function  $\lambda(t|\mathcal{H}_t)$  conditioned on the history  $\mathcal{H}_t$  of the

301 process itself. Hence, we have:

$$302 \quad \lambda(t|\mathcal{H}_t) = \exp \left\{ \nu + \beta [X_0 + \rho t - \sum_{i:t_i < t} X_i] \right\} \quad (13)$$

303 where  $X_i$  is the strain  $X_B$  (8), the seismic moment  $X_M$  (9), the seismic energy  $X_E$  (10), or  
 304 the scaled energy  $X_S$  (11), depending on the version of the SR model under examination.  
 305 The quantity  $X_i$  is released at time  $t_i$  by an earthquake where the magnitude is scaled by  
 306 a threshold magnitude  $M_{th}$ . The rupture area involved in the expression of the seismic  
 307 energy (5) and the scaled energy (7) is obtained as a function of the earthquake moment  
 308 magnitude, by the regression  $\log_{10} A_w = a + b M_w$  (Wells & Coppersmith, 1994), where the  
 309 parameters  $a$  and  $b$  depend on the faulting type of the associated fault source. Specifically,  
 310  $a = -2.87$  and  $b = 0.82$  for normal fault (N),  $a = -3.99$  and  $b = 0.98$  for reverse fault (R),  
 311  $a = -3.42$  and  $b = 0.90$  for left/right-lateral strike-slip fault (LL/RL); Figure 4 represents  
 312 the four proxy measures of the stress versus moment magnitude by taking into account  
 313 the faulting types. Tables 1 and 2 provide the faulting types of each fault source.

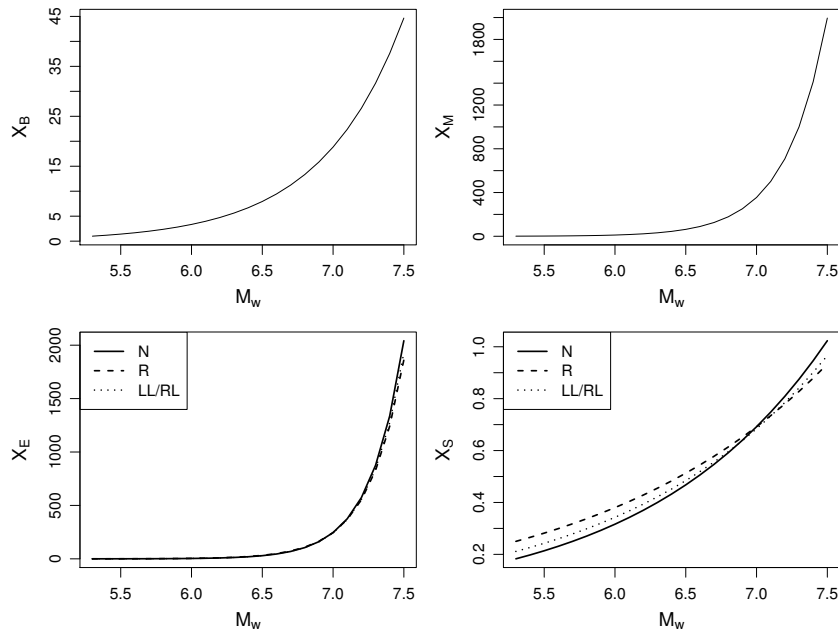


Figure 4: The strain  $X_B$  (top-left), the seismic moment  $X_M$  (top-right), the seismic energy  $X_E$  (bottom-left), and the scaled energy  $X_S$  (bottom-right) versus moment magnitude, where  $X_E$  and  $X_S$  are provided for different faulting types.

314 The parameter vector to be estimated is  $\theta = (\alpha, \beta, \rho)$  where  $\alpha = \nu + \beta X_0$  (see Equation  
 315 (13)). According to the Bayesian paradigm, we assume the model parameters  $\theta$  as random  
 316 variables and formalize our beliefs about their variability, borrowed from the literature and  
 317 previous experience, through prior distributions (e.g., as for the original version of the SR  
 318 model, see Votsi et al. 2011; Jiang et al. 2011; Rotondi & Varini 2007). In our case, this  
 319 information is not available because the SR model is here formulated in terms of moment  
 320 and energy for the first time; moreover, the parameters  $\alpha, \beta, \rho$  are not strictly related to  
 321 easily measurable physical quantities. We then assign the prior distributions according to  
 322 an objective Bayesian perspective, by combining the empirical Bayes method (Carlin &  
 323 Louis, 2000) and the use of vague-proper prior distributions (Berger, 2006). We choose  
 324 the families of the prior distributions according to the support of the parameters ( $\beta$  and  
 325  $\rho$  are positive parameters, and  $\alpha$  lies on the real line), and we set the prior parameters  
 326 (called *hyperparameters*) equal to the prior mean and variance of the corresponding model  
 327 parameter; for instance,  $\beta$  follows *a priori* the Gamma distribution  $Gamma(\xi, \nu)$  where  
 328  $\xi = E_0(\beta)$  and  $\nu = \text{var}_0(\beta)$ . According to the empirical Bayes method, preliminary values  
 329 of the hyperparameters  $\eta$  are obtained by maximizing the marginal likelihood:

$$330 \quad \eta_{\mathbf{EB}} = \arg \max_{\eta \in H} m(\text{data} | \eta) = \arg \max_{\eta \in H} \int_{\theta \in \Theta} \mathcal{L}(\text{data} | \theta) \pi_0(\theta | \eta) d\theta \quad (14)$$

331 and by setting the standard deviations to 90% of the corresponding means, to avoid the  
 332 estimates provided for the variances through the maximization (14) being too close to zero.  
 333 This procedure clearly implies a double use of the data: in assigning the hyperparameters  
 334 and in evaluating the posterior distributions. This philosophically undesirable double use  
 335 can become a serious issue when the sample size is fairly small, as in our case. A solution  
 336 is provided by choosing priors that ‘span the range of the likelihood function’ (Berger,  
 337 2006); that is, by varying the hyperparameters around their preliminary estimates  $\eta_{\mathbf{EB}}$   
 338 and choosing those values that include most of the mass of the likelihood function, but  
 339 that do not extend too far. For a graphic exemplification of this procedure we refer to  
 340 Varini & Rotondi (2015).

341 In the Bayesian framework, the prior distribution of the parameter  $\theta$  is given by  $\pi_0$ ,

342 and the log likelihood function is given by:

$$343 \quad \log \mathcal{L}(data | \theta) = \sum_{i=1}^N \log \lambda(t_i) - \int_{T_c}^{T_f} \lambda(s) ds. \quad (15)$$

344 Through Bayes' theorem, the posterior distribution is given as:

$$345 \quad \pi(\theta | data) = \frac{\mathcal{L}(data | \theta) \pi_0(\theta)}{\int_{\Theta} \mathcal{L}(data | \theta) \pi_0(\theta) d\theta} \quad (16)$$

346 from which the estimate of the parameter can be obtained, which is typically given by the  
347 posterior mean, and measures of its uncertainty expressed through measures of location  
348 (median and mode), dispersion (variance and quantiles), and shape of the distribution  
349 (skewness and kurtosis). The explicit formulation of the posterior distribution generally  
350 requires the computation of multi-dimensional integrals. This can seldom be done in the  
351 closed form; numerical methods on integral approximations are a standard solution for  
352 this problem. Recently, methods based on the stochastic simulation of Markov chains  
353 have turned out to be highly efficient and flexible tools. MCMC methods are a class of  
354 algorithms for sampling from probability distributions, which are based on constructing  
355 a Markov chain that has the desired distribution as its equilibrium distribution. The  
356 states of the chain after a large number of steps can be used as samples from the desired  
357 distribution. In the Bayesian context, the target distribution is the posterior distribution  
358 of the parameter  $\theta$ . The algorithm applied to generate the Markov chains is summarized  
359 in Appendix B. Then diagnostic tools are applied to the sequences of the values generated  
360 for each parameter through pilot runs of the estimation algorithm, to test if it is safe to  
361 stop sampling and to use those sequences to estimate the characteristics of the posterior  
362 distributions, or if necessary, to vary the variance of the proposal distribution to reach  
363 the optimal acceptance rate so that a long run of the MCMC algorithm guarantees the  
364 best estimates for the model parameters.

## 365 4.2 Model comparison

366 We provide an overview of the approaches for model comparison that are then applied in  
367 Section 5: the Bayes factor, the Ando & Tsay information criterion, and a retrospective  
368 analysis based on the probability distribution of the waiting time for the next event that  
369 is obtained from the SR model.

### 370 4.2.1 Bayes factor

371 We adopt the Bayesian approach to quantify the evidence in favor of one model in pairs of  
372 candidate models, through the Bayes factor. Given the models  $\mathcal{M}_1$ ,  $\mathcal{M}_2$ , and the dataset  
373  $\mathbf{D}$ , the Bayes factor is the ratio of the posterior odds of  $\mathcal{M}_1$  to its prior odds; that is to  
374 say:

$$375 B_{12} = \frac{pr(\mathbf{D} | \mathcal{M}_1)}{pr(\mathbf{D} | \mathcal{M}_2)} = \frac{pr(\mathcal{M}_1 | \mathbf{D})}{pr(\mathcal{M}_2 | \mathbf{D})} \div \frac{pr(\mathcal{M}_1)}{pr(\mathcal{M}_2)} \quad (17)$$

376 When the prior probabilities of the two competing hypotheses are equal, the Bayes factor  
377 coincides with the posterior odds. The densities  $pr(\mathbf{D} | \mathcal{M}_k)$ ,  $k = 1, 2$  are obtained by  
378 integrating over the parameter space with respect to their prior distributions:

$$379 pr(\mathbf{D} | \mathcal{M}_k) = \int pr(\mathbf{D} | \theta_k, \mathcal{M}_k) \pi(\theta_k | \mathcal{M}_k) d\theta_k \quad (18)$$

380 where  $\pi(\theta_k | \mathcal{M}_k)$  is the prior density of the parameter  $\theta_k$  under  $\mathcal{M}_k$ , and  $pr(\mathbf{D} | \theta_k, \mathcal{M}_k)$   
381 is the likelihood function of  $\theta_k$ . The quantity  $pr(\mathbf{D} | \mathcal{M}_k)$  is a *marginal* (or *integrated*)  
382 *likelihood*; it is also referred to as *evidence* for  $\mathcal{M}_k$ . Details on the computational aspects  
383 concerning the evaluation of the Bayes factor can be found in Rotondi & Varini (2007).

### 384 4.2.2 Ando and Tsay information criterion

385 For each model, the Bayes factor considers the posterior probability induced by the prior  
386 distribution  $\pi(\theta)$ , and aims at the model comparison by looking for the best fit of the  
387 model to the data. Alternatively, one may be interested in the predictions from the various  
388 models and in choosing which model gives the best predictions of future observations  
389 generated by the same process as the original data. The predictive performance of a

390 model  $\mathcal{M}_k$  is assessed by scoring rules (Gneiting & Raftery , 2007); the most commonly  
 391 used is the logarithmic score derived from the Kullback-Leibler distance between two  
 392 distributions, the predictive distribution for new data  $\mathbf{z}$  given the observations  $\mathbf{y}$  and  
 393 their true density  $g(\mathbf{z})$ :

$$\begin{aligned}
 394 \quad & \int \left[ \log \frac{g(\mathbf{z}_n)}{pr(\mathbf{z}_n | \mathbf{y}_n, \mathcal{M}_k)} \right] g(\mathbf{z}_n) d\mathbf{z}_n \\
 395 \quad & = \int \log[g(\mathbf{z}_n)] g(\mathbf{z}_n) d\mathbf{z}_n - \int \log pr(\mathbf{z}_n | \mathbf{y}_n, \mathcal{M}_k) g(\mathbf{z}_n) d\mathbf{z}_n. \quad (19)
 \end{aligned}$$

396 The term relevant to the model  $\mathcal{M}_k$  is the latter, which is the expected log-predictive  
 397 likelihood where the unknown true density can be approximated by the empirical distri-  
 398 bution  $\tilde{g}(\mathbf{y}_n)$  constructed by the data so as to obtain as estimator the posterior predictive  
 399  $\frac{1}{n} \log pr(\mathbf{y}_n | \mathbf{y}_n, \mathcal{M}_k)$ . The accuracy of the predictions of future data is generally lower  
 400 than the accuracy of the predictions of the same model for the observed data; then the  
 401 resulting overestimation has to be corrected by applying some sort of bias correction. Fol-  
 402 lowing this approach, a variety of measures of predictive accuracy have been proposed in  
 403 the literature, which are also referred to as information criteria; for instance, the Akaike  
 404 information criterion (AIC) adopts the maximum likelihood estimate for  $\theta$ , whereas the  
 405 deviance criterion (DIC) uses the posterior mean  $E(\theta | \mathbf{y}_n)$ ; for a review, we refer the  
 406 reader to Vehtari & Ojanen (2012).

407 The Watanabe criterion (Watanabe , 2010) has the advantage of being fully Bayesian,  
 408 because it averages the predictive distribution over the posterior distribution  $\pi(\theta|\mathbf{y}_n)$   
 409 rather than conditioning on a point estimate. However, it is hardly applicable to data  
 410 that, as in our case, are not independent given parameters. A solution is given by the  
 411 Ando & Tsay criterion where the joint density can be decomposed into the product of  
 412 the conditional densities  $pr(\mathbf{y}_n | \theta) = \prod_{i=1}^n pr(y_i | y_{(1:i-1)}, \theta)$  (Ando & Tsay 2010, pgg.  
 413 747-748). The complete definition of this criterion is the following:

$$414 \quad PL(\mathcal{M}_k) = \frac{1}{n} \left( \int \log pr(\mathbf{y}_n | \theta, \mathcal{M}_k) \pi(\theta|\mathbf{y}_n) d\theta - \frac{p}{2} \right), \quad (20)$$

415 where, in the bias correction,  $p$  is the dimension of  $\theta$  and the integral can be evaluated

416 using draws from the posterior  $\pi(\theta|\mathbf{y}_n)$  performed in the MCMC estimation procedure, so  
 417 that we have:

$$418 \quad PL(\mathcal{M}_k) = \frac{1}{n} \left\{ \log \left( \frac{1}{R} \sum_{j=1}^R pr(\mathbf{y}_n | \theta^{(j)}, \mathcal{M}_k) \right) - \frac{p}{2} \right\}. \quad (21)$$

419 To be on the same scale as the other criteria, we multiply Equation (21) by  $-2n$ .

### 420 4.2.3 Probability distribution of the ‘time to next event’

421 For a more detailed analysis of the model performance we derive the probability distri-  
 422 bution of the time to the next event for each class of SR model in an explicit way. This  
 423 enables us to perform a retrospective analysis by comparing the occurrence time of each  
 424 earthquake with its forecast value from the model. At the instant  $t$ , let us consider the  
 425 conditional intensity function:

$$426 \quad \lambda(t|\mathcal{H}_t) = \exp \{ \alpha + \beta[\rho t - S(t)] \} \quad (22)$$

427 of the general SR model with parameter vector  $\theta = (\alpha, \beta, \rho)$ . Let  $W_t$  be the random  
 428 waiting time for the next event given the history  $\mathcal{H}_t$  up to  $t$ ; hence, the occurrence time  
 429 of the next event will be  $T = t + W_t$ . Hereinafter, for the sake of simplicity, we substitute  
 430 the explicit indication of the conditioning on  $\mathcal{H}_t$  with the subscript  $t$ .

431 The conditional cumulative distribution of  $W_t$  is given by:

$$432 \quad \begin{aligned} F_t(w | \theta) &= Pr(W_t \leq w | \theta) = 1 - Pr(W_t > w | \theta) = 1 - Pr(N_{t+w} - N_t = 0 | \theta) \\ 433 \quad &= 1 - \exp \left( - \int_t^{t+w} \lambda(u) du \right) \\ 434 \quad &= 1 - \exp \left[ - \frac{1}{\beta\rho} \left( e^{\alpha + \beta(\rho(t+w) - S(t))} - e^{\alpha + \beta(\rho t - S(t))} \right) \right] \quad (23) \\ 435 \quad &= 1 - \exp \left[ - \frac{\lambda(t)}{\beta\rho} (e^{\beta\rho w} - 1) \right], \end{aligned}$$

436 where  $N_s$  is the number of earthquakes recorded by time  $s$ . If we set  $\phi_t = \lambda(t)/(\beta\rho)$  and

437  $\eta = \beta\rho$ , then we have:

$$438 \quad F_t(w | \theta) = 1 - \exp\{-\phi_t (e^{\eta w} - 1)\}, \quad (24)$$

439 which is a Gompertz distribution with shape parameter  $\phi_t > 0$ , scale parameter  $\eta > 0$ ,  
 440 and support  $w \geq 0$ . As the probability that an event occurs before a fixed time  $w$  increases  
 441 with  $\phi_t$ , the shape parameter  $\phi_t$  can be interpreted as the propensity of the region to the  
 442 occurrence. The probability density function is such that:

$$443 \quad f_t(w | \theta) = \eta\phi_t e^{\eta w} e^{\phi_t} \exp(-\phi_t e^{\eta w}). \quad (25)$$

444 This function can take a large variety of shapes, and be skewed either to the right or  
 445 the left. To describe the characteristics of the Gompertz distribution (24), we recall its  
 446 summary statistics: mode, mean, variance, and quartiles (Lenart , 2014). The mode of  
 447 the density function (25) is as follows:

$$448 \quad w^* = \begin{cases} \frac{1}{\eta} \log \frac{1}{\phi_t}, & \text{with } 0 < F(w^*) < 1 - e^{(-1)} = 0.632 & \text{if } 0 < \phi_t < 1 \\ 0 & & \text{if } \phi_t \geq 1. \end{cases} \quad (26)$$

449 The expected waiting time for the future event is such that:

$$450 \quad E(W_t | \theta) = -\frac{e^{\phi_t}}{\eta} \text{Ei}(-\phi_t), \quad (27)$$

451 where  $\text{Ei}()$  is the exponential integral  $\text{Ei}(x) = -\int_{-x}^{\infty} (e^{-u}/u) du$ , (Abramowitz & Stegun  
 452 1972, p. 228). On the one hand, according to the Reid theory, when  $\phi_t$  (or equivalently  
 453  $\lambda(t)$ ) gets close to 0, Equation (27) approaches  $\infty$ ; i.e., after a large reduction in the  
 454 hazard function  $\lambda(\cdot)$  due to a very high ‘stress’ release, an unusually long waiting time  
 455 should elapse before the next event. On the other hand, the expected waiting time can  
 456 be short even when it is evaluated after relatively large earthquakes, because through  
 457 the parameter  $\phi_t$  it depends on the value that the hazard function has at the occurrence  
 458 time. Indeed, if an earthquake of size  $X_i$  occurs at time  $t_i$ , the drop of the hazard



459 function,  $\Delta\lambda(t_i) = \lambda(t_i^-) [\exp(-\beta X_i) - 1]$ , depends on the value of the hazard function  
460  $\lambda(t_i^-)$  computed immediately before the occurrence time. Consequently, variations in the  
461 hazard function caused by two events of the same size, but that occurred at different  
462 times, are typically different; hence, depending on the conditions of the system at that  
463 moment, the SR model does not preclude a small waiting time, even immediately after a  
464 strong event.

465 The variance of  $W_t$  is such that:

$$\begin{aligned}
V(W_t | \theta) &= \frac{1}{\eta^2} \int_0^1 \log^2 \left( 1 - \frac{\log u}{\phi_t} \right) du - [E(W_t | \theta)]^2 \\
&= \frac{\phi_t e^{\phi_t}}{\eta^2} \left\{ \frac{(\log^2 \phi_t + 2\gamma \log \phi_t + \pi^2/6 + \gamma^2)}{\phi_t} - 2 {}_3F_3 \left[ \begin{matrix} 1, 1, 1 \\ 2, 2, 2 \end{matrix}; -\phi_t \right] \right\} - [E(W_t | \theta)]^2
\end{aligned} \tag{28}$$

467 where  $\gamma = 0.5772\dots$  is the Euler-Mascheroni constant, and  ${}_3F_3$  is the generalized hyper-  
468 geometric function.

469 The generic quantile of order  $q$  is given by  $W_q = \eta^{-1} \log(1 - \phi_t^{-1} \log(1 - q))$ ; hence, the  
470 median is equal to  $\eta^{-1} \log(1 - \phi_t^{-1} \log 0.5)$ . Consistent with the definition of conditional  
471 intensity function, the hazard rate holds that  $h_t(w | \theta) = f_t(w | \theta) / [1 - F_t(w | \theta)] =$   
472  $\phi_t \eta e^{\eta w} = \lambda(t) e^{\eta w} = \lambda(t + w)$ , and hence it is an exponential increasing function.

473 In the case where additional time  $h$  has elapsed after the issue time  $t$  of the forecast,  
474 and no event has occurred during that time  $h$ , the distributions of the waiting times  $W_t$   
475 and  $W_{t+h}$  can be compared. The second distribution is thus issued at time  $(t + h)$ , and it  
476 is enriched by the additional knowledge that no event has occurred between  $t$  and  $t + h$ .  
477 Since  $\phi_{t+h} = \phi_t e^{\eta h} \geq \phi_t$  for all  $h > 0$ , the expected value of the waiting time  $W_{t+h}$   
478 decreases as  $h$  increases; that is,  $E(W_t | \theta) \geq E(W_{t+h} | \theta)$ :

$$\begin{aligned}
E(W_t | \theta) &= -\frac{e^{\phi_t}}{\eta} \text{Ei}(-\phi_t) = \frac{e^{\phi_t}}{\eta} \int_{\phi_t}^{+\infty} \frac{e^{-u}}{u} du \stackrel{[u=\phi_t(z+1)]}{=} \frac{1}{\eta} \int_0^{+\infty} \frac{e^{-\phi_t z}}{z+1} dz \geq \\
&\geq \frac{1}{\eta} \int_0^{+\infty} \frac{e^{-\phi_{t+h} z}}{z+1} dz = E(W_{t+h} | \theta).
\end{aligned} \tag{29}$$

480 Moreover, it holds (Abramowitz & Stegun 1972, p. 229) that:

$$481 \quad \frac{1}{2\eta} \ln \left( 1 + \frac{2}{\phi_{t+h}} \right) < E(W_{t+h} | \theta) < \frac{1}{\eta} \ln \left( 1 + \frac{1}{\phi_{t+h}} \right). \quad (30)$$

482 Therefore, as  $\phi_{t+h}$  tends to infinity as  $h$  increases, the expected waiting time tends to  
 483 zero as  $h$  grows to infinity and approaches its limit, with a convergence rate of  $O(e^{-\eta h})$ .

484 Similarly, it can be shown that also the variance decreases to zero when  $h$  tends to infinity.

485 For more details on the Gompertz distribution and further consideration of its application  
 486 to other SR models we refer the reader to Varini & Rotondi (2015)

487 We recall that the Bayesian approach not only provides a point estimate of the parameters,  
 488 but also a measure of their uncertainty in terms of the posterior distribution. Taking into  
 489 account this uncertainty, the posterior predictive distribution of  $W_t$  is given by:

$$490 \quad F_t(w) = P(W_t < w) = \int_{\Theta} P(W_t < w | \theta) \pi(\theta | data) d\theta, \quad (31)$$

491 where the conditional Gompertz distribution of  $W_t$  is integrated with respect to the poste-  
 492 rior distribution of the parameters. Pointwise approximation of the resulting probability  
 493 distribution can be obtained by varying the model parameters into the Markov chains  
 494 generated for their estimation (see Section 4.1):

$$495 \quad F_t(w) \approx \hat{F}_t(w) = \frac{\sum_{j=1}^R P(W_t < w | \theta^{(j)})}{R}. \quad (32)$$

496 The expected value of the waiting time  $W_t$  is estimated by the average of the expected  
 497 waiting times  $E(W_t | \theta^{(j)})$ ,  $j = 1, \dots, R$ , as given by (27); similarly for the variance of  $W_t$ ,  
 498 as the  $\theta^{(j)}$  have negligible correlation, as indicated by the diagnostics on the convergence  
 499 of the Markov chains. The mode of  $W_t$  can be evaluated through a numerical optimization  
 500 algorithm (e.g., we use the direct search complex algorithm), which finds the waiting time  
 501 in which the posterior predictive density function of  $W_t$  reaches the global maximum.  
 502 The quantile of order  $q$  is the solution  $w_q$  of the equation  $\hat{F}_t(w) = q$ ; we have solved this  
 503 by the Müller method, as implemented in IMSL numerical libraries, version 4.0 (IMSL

504 , 2000). Through the quantiles, we then estimate the Highest Posterior Density (HPD)  
505 (or credible) interval of order  $q$  ( $0 < q < 1$ ) for the waiting time  $W_t$ , which is the time  
506 interval that satisfies the following two conditions: (a) the probability of that interval is  
507  $q$ ; and (b) the lowest density of any point within that interval is greater than or equal  
508 to the density of any point outside the interval. In other words, the most likely waiting  
509 times belong to the HPD interval, which turns out to be the smallest interval of order  $q$ .

510 The relationship  $T = t + W_t$  links the time of the next event  $T$  with the corresponding  
511 waiting time  $W_t$ , and allows the estimation of the distribution  $F(\cdot)$  of  $T$  and its summary  
512 statistics, so that it is possible to perform both retrospective and prospective validations.

## 513 **5 Results**

514 This section illustrates the results concerning both the parameter estimations and model  
515 comparisons related to the application of the four versions of the SR model to the data  
516 of each MR.

### 517 **5.1 Parameter estimates**

518 Details on the prior distributions used in the Bayesian inferential procedure are reported  
519 in Table B2. As illustrative examples, the prior and posterior densities of the parameters  
520 of the four models for MR<sub>3</sub> and MR<sub>4</sub> are shown in Figures B1 and B2, respectively.  
521 Table 5 collects parameter estimates of the different models obtained through the MCMC  
522 algorithm by generating a chain of  $R = 250,000$  elements, after discarding 50,000 elements  
523 as burn-in, and recording the output every 20th iteration, for each parameter.

524 The  $\alpha$  parameters for the four models of each MR are similar, and according to the  
525 order of their size, they are equal to the natural logarithm of the average number of events  
526 per year. The  $\rho$  parameters vary according to the stress proxy used in the model. Thus,  
527 e.g., in MR<sub>4</sub>, for the middle value of the magnitude  $M_w = 6.4$ , the values of  $X_B$ ,  $X_E$ ,  
528 and  $X_S$  are about 16%, 42%, and 1%, respectively, of the value of  $X_M$ ; analogously  $\hat{\rho}_B$ ,  
529  $\hat{\rho}_E$ , and  $\hat{\rho}_S$  are 13.6%, 62%, and 1.3%, respectively, of  $\hat{\rho}_M = 2.55$ . As  $\beta$  and  $\rho$  behave

530 inversely,  $\hat{\beta}_E$  has the same order of size of  $\hat{\beta}_M$ , whereas  $\hat{\beta}_B$  and  $\hat{\beta}_S$  increases by one and  
531 two orders with respect  $\hat{\beta}_M$ .

	<b>R<sub>B</sub></b>			<b>R<sub>M</sub></b>		
	$\hat{\alpha}$	$\hat{\beta}$	$\hat{\rho}$	$\hat{\alpha}$	$\hat{\beta}$	$\hat{\rho}$
MR <sub>1</sub>	-5.65	3.14E-1	5.33E-2	-7.29	2.20E-1	1.38E-1
MR <sub>2</sub>	-2.83	6.64E-2	1.66E-1	-2.87	1.09E-2	6.03E-1
MR <sub>3</sub>	-1.72	3.02E-2	2.93E-1	-1.62	1.04E-2	6.04E-1
MR <sub>4</sub>	-1.98	2.11E-2	3.48E-1	-2.02	1.21E-3	2.55
MR <sub>5</sub>	-2.51	6.23E-2	2.26E-1	-2.57	3.78E-3	1.40
MR <sub>6</sub>	-2.57	4.24E-2	2.66E-1	-2.58	3.49E-3	2.90
MR <sub>7</sub>	-2.14	6.67E-3	6.36E-1	-2.18	3.56E-4	8.45
MR <sub>8</sub>	-3.24	1.39E-2	2.69E-1	-2.18	3.51E-4	8.73
	<b>R<sub>E</sub></b>			<b>R<sub>S</sub></b>		
	$\hat{\alpha}$	$\hat{\beta}$	$\hat{\rho}$	$\hat{\alpha}$	$\hat{\beta}$	$\hat{\rho}$
MR <sub>1</sub>	-7.17	7.56E-1	4.24E-2	-4.96	1.38	7.31E-3
MR <sub>2</sub>	-2.84	1.83E-2	2.47E-1	-2.92	9.92E-1	2.33E-2
MR <sub>3</sub>	-1.63	2.30E-2	2.12E-1	-1.80	1.89E-1	5.20E-2
MR <sub>4</sub>	-2.08	1.67E-3	1.59	-2.13	5.36E-1	3.31E-2
MR <sub>5</sub>	-2.59	7.15E-3	6.96E-1	-2.45	1.63	2.27E-2
MR <sub>6</sub>	-2.60	6.28E-3	1.68	-2.62	1.05	1.66E-2
MR <sub>7</sub>	-2.19	4.44E-4	5.88	-2.17	1.70E-1	4.44E-2
MR <sub>8</sub>	-3.27	3.72E-4	8.35	-3.61	7.89E-1	1.71E-2

Table 5: Parameter estimates for the **R<sub>B</sub>**, **R<sub>M</sub>**, **R<sub>E</sub>**, and **R<sub>S</sub>** models in each MR.

532 As an example, Figures 5 and 6 show the results for the estimate of the conditional  
533 intensity function that is obtained by applying the various models to the data from MR<sub>3</sub>  
534 and MR<sub>4</sub>, which can be followed in two ways. The first is to replace the parameter  
535 estimates in the different versions of the expression (2), thereby obtaining the so-called  
536 plug-in estimate  $\tilde{\lambda}(t) = \lambda(t | \hat{\theta}, \mathcal{H}_T)$ , where  $\hat{\theta}$  is the vector of posterior means. The second  
537 way is to estimate the conditional intensity through the ergodic mean  $\hat{\lambda}(t) = \frac{1}{R} \sum_{j=1}^R \lambda(t |$   
538  $\theta^{(j)}, \mathcal{H}_T)$ , where  $\theta^{(j)}$  is the  $j$ th element of the Markov chain generated for each parameter  
539 by the MCMC algorithm. Through the sequence  $\{\lambda(t | \theta^{(j)}, \mathcal{H}_T)\}_{j=1}^R$ , we can also obtain  
540 the median and quartiles of the pointwise estimate  $\hat{\lambda}(t)$ .

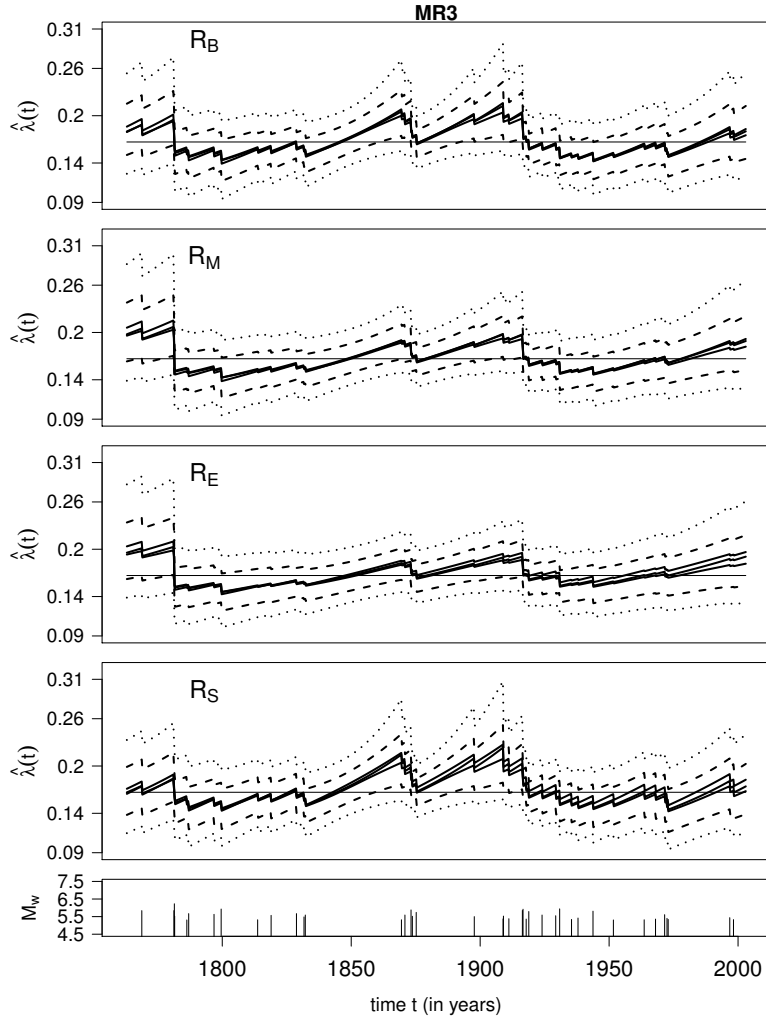


Figure 5: Conditional intensity function of the  $\mathbf{R}_B$ ,  $\mathbf{R}_M$ ,  $\mathbf{R}_E$ , and  $\mathbf{R}_S$  models. The ergodic mean, plug-in estimate, and median are all represented by solid lines that are practically indistinguishable from each other; 1<sup>st</sup> and 3<sup>rd</sup> quartiles (dashed line), 10% and 90% quantiles (dotted line). The Poisson rate is shown for comparison (horizontal thin line). The bottom panel shows the time history of the earthquakes scaled by their moment magnitudes ( $M_w$ ). The example is taken from  $MR_3$ .

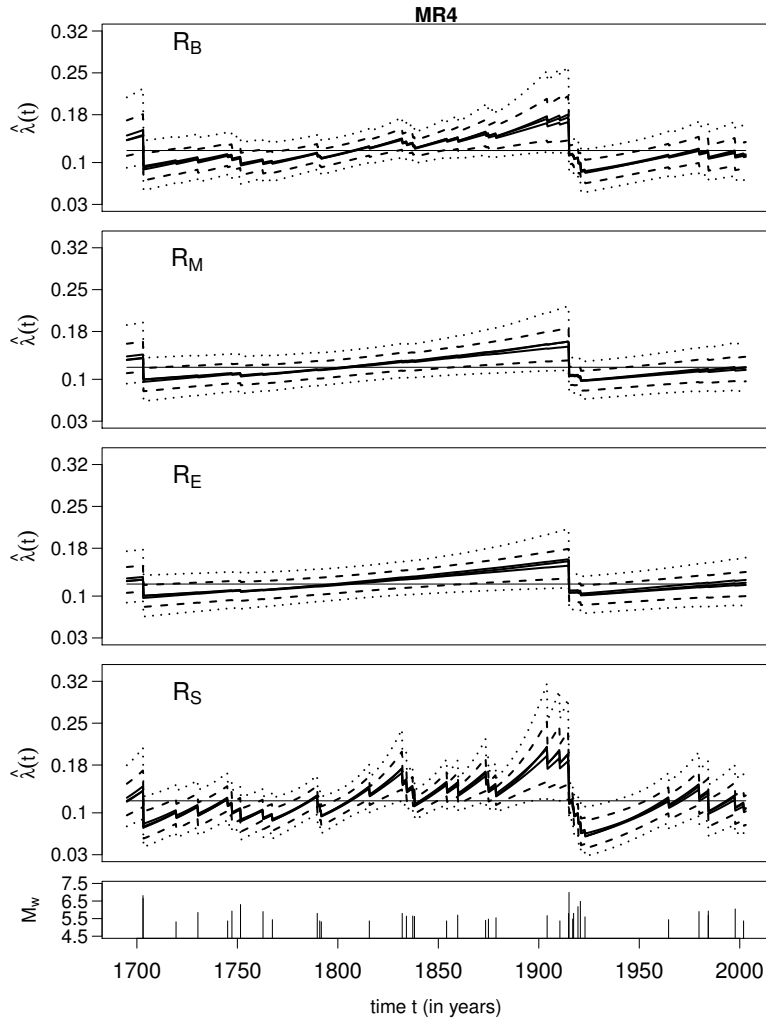


Figure 6: Same as Figure 5. The example is taken from  $MR_4$ .

## 541 5.2 Results of the model comparison

542 In this Section, we compare the four versions of the SR model to identify the best one; we  
543 note that what constitutes the “best” model is not uniquely defined, as it often depends  
544 on the goals of the user. Model testing can be performed for different purposes, such as  
545 the goodness of fit to the data of the learning set and the forecasting skill. To reach these  
546 aims, we propose two validation criteria: the Bayes factor that compares pairwise models  
547 through the ratio of their marginal densities with respect to the prior distributions of the  
548 parameters, and the information criterion by Ando and Tsay that averages the predictive  
549 distributions over the posterior distributions of the parameters.

550 **5.2.1 Bayes factor**

551 Table 6 shows the marginal  $\log_{10}$  likelihood of each model, as applied to the various MRs,  
 552 under the assumption that the prior probabilities of the models are equal; the maximum  
 553 value represents the best model. In six out of eight MRs, the highest value is given by  
 554 model  $\mathbf{R}_S$ , and in the remaining ones by model  $\mathbf{R}_E$ .

model region	$R_B$	$R_M$	$R_E$	$R_S$
MR <sub>1</sub>	-15.1469	-13.8686	<b>-13.5957</b>	-15.6580
MR <sub>2</sub>	-27.3373	-27.5929	-27.5686	<b>-27.1243</b>
MR <sub>3</sub>	-49.6949	-49.7956	<b>-48.9883</b>	-49.7344
MR <sub>4</sub>	-50.3988	-50.6119	-50.6318	<b>-50.1548</b>
MR <sub>5</sub>	-21.9602	-22.0761	-22.1250	<b>-21.4926</b>
MR <sub>6</sub>	-28.2593	-28.2575	-28.2209	<b>-28.1026</b>
MR <sub>7</sub>	-43.1532	-43.1471	-43.0928	<b>-43.0173</b>
MR <sub>8</sub>	-35.3877	-35.4283	-35.3487	<b>-35.0062</b>

Table 6: Marginal  $\log_{10}$  likelihood for the four stress release model versions. Bold: the maximum value, which indicates the best model in each MR.

555 More specifically, to evaluate the significance of these results, Table 7 shows the set  
 556 of pairwise Bayes factors for each MR: according to the interpretation of Jeffreys' scale  
 557 given by Kass & Raftery (1995), values in the three ranges of (0, 0.5), (0.5, 1), and (1,  
 558 2) of the  $\log_{10} B_{12}$  indicate 'barely worth mentioning', 'positive', and 'strong' evidence,  
 559 respectively, in favor of the model  $\mathcal{M}_1$ . Based on the Bayes factors, it can be seen that:

560 In MR<sub>1</sub>,  $\mathbf{R}_E$  behaves similarly to  $\mathbf{R}_M$  ( $\log_{10} B_{EM} = 0.27$  means that the evidence  
 561 in favour of  $\mathbf{R}_E$  is barely worth mentioning), whereas  $\mathbf{R}_E$  shows strong evidence  
 562 against  $\mathbf{R}_B$  and  $\mathbf{R}_S$ ;

563 In MR<sub>2</sub>, there is slight evidence in favor of  $\mathbf{R}_S$  compared to the other models, while  
 564  $\mathbf{R}_M$  shows the worst performance;

565 In MR<sub>3</sub>,  $\mathbf{R}_E$  shows positive evidence against the other models, with  $\mathbf{R}_M$  being the  
 566 worst again;

567 In  $MR_4$ , there is slight evidence in favor of  $\mathbf{R}_S$  compared to the other models, while  
568  $\mathbf{R}_E$  shows the worst performance;

569 In  $MR_5$ ,  $\mathbf{R}_S$  performs from slightly-to-moderately better than the other models;  $\mathbf{R}_E$   
570 shows the worst performance;

571 In  $MR_6$ , there is minimal evidence in favor of  $\mathbf{R}_S$ , and minimal evidence against  
572  $\mathbf{R}_B$ ;

573 In  $MR_7$ , as in  $MR_6$ ;

574 In  $MR_8$ ,  $\mathbf{R}_S$  performs slightly better than the other models, with  $\mathbf{R}_M$  being the  
575 worst.



		MR <sub>1</sub>			
$\mathcal{M}_1 \backslash \mathcal{M}_2$		$R_B$	$R_M$	$R_E$	$R_S$
$R_B$		-	-1.2784	-1.5512	<b>0.5111</b>
$R_M$		<b>1.2784</b>	-	-0.2728	<b>1.7894</b>
$R_E$		<b>1.5512</b>	<b>0.2728</b>	-	<b>2.0623</b>
$R_S$		-0.5111	-1.7894	-2.0623	-

		MR <sub>2</sub>			
$\mathcal{M}_1 \backslash \mathcal{M}_2$		$R_B$	$R_M$	$R_E$	$R_S$
$R_B$		-	<b>0.2556</b>	<b>0.2314</b>	-0.2130
$R_M$		-0.2556	-	-0.0243	-0.4686
$R_E$		-0.2314	<b>0.0243</b>	-	-0.4443
$R_S$		<b>0.2130</b>	<b>0.4686</b>	<b>0.4443</b>	-

		MR <sub>3</sub>			
$\mathcal{M}_1 \backslash \mathcal{M}_2$		$R_B$	$R_M$	$R_E$	$R_S$
$R_B$		-	<b>0.1007</b>	-0.7067	<b>0.0394</b>
$R_M$		-0.1007	-	-0.8073	-0.0612
$R_E$		<b>0.7067</b>	<b>0.8073</b>	-	<b>0.7461</b>
$R_S$		-0.0394	<b>0.0612</b>	-0.7461	-

		MR <sub>4</sub>			
$\mathcal{M}_1 \backslash \mathcal{M}_2$		$R_B$	$R_M$	$R_E$	$R_S$
$R_B$		-	<b>0.2131</b>	<b>0.2330</b>	-0.2440
$R_M$		-0.2131	-	<b>0.0199</b>	-0.4571
$R_E$		-0.2330	-0.0199	-	-0.4770
$R_S$		<b>0.2440</b>	<b>0.4571</b>	<b>0.4770</b>	-

		MR <sub>5</sub>			
$\mathcal{M}_1 \backslash \mathcal{M}_2$		$R_B$	$R_M$	$R_E$	$R_S$
$R_B$		-	<b>0.1159</b>	<b>0.1648</b>	-0.4676
$R_M$		-0.1159	-	<b>0.0489</b>	-0.5835
$R_E$		-0.1648	-0.0489	-	-0.6324
$R_S$		<b>0.4676</b>	<b>0.5835</b>	<b>0.6324</b>	-

		MR <sub>6</sub>			
$\mathcal{M}_1 \backslash \mathcal{M}_2$		$R_B$	$R_M$	$R_E$	$R_S$
$R_B$		-	-0.0018	-0.0384	-0.1567
$R_M$		<b>0.0018</b>	-	-0.0366	-0.1549
$R_E$		<b>0.0384</b>	<b>0.0366</b>	-	-0.1184
$R_S$		<b>0.1567</b>	<b>0.1549</b>	<b>0.1184</b>	-

		MR <sub>7</sub>			
$\mathcal{M}_1 \backslash \mathcal{M}_2$		$R_B$	$R_M$	$R_E$	$R_S$
$R_B$		-	-0.0061	-0.0603	-0.1358
$R_M$		<b>0.0061</b>	-	-0.0542	-0.1297
$R_E$		<b>0.0603</b>	<b>0.0542</b>	-	-0.0755
$R_S$		<b>0.1358</b>	<b>0.1297</b>	<b>0.0755</b>	-

		MR <sub>8</sub>			
$\mathcal{M}_1 \backslash \mathcal{M}_2$		$R_B$	$R_M$	$R_E$	$R_S$
$R_B$		-	<b>0.0406</b>	-0.0389	-0.3815
$R_M$		-0.0406	-	-0.0796	-0.4221
$R_E$		<b>0.0389</b>	<b>0.0796</b>	-	-0.3425
$R_S$		<b>0.3815</b>	<b>0.4221</b>	<b>0.3425</b>	-

Table 7: Bayes factors  $\log_{10} B_{12}$  comparisons of the four stress release models, pair by pair ( $M_1$  vs  $M_2$ ), in every MR. Jeffreys' scale is used for rating the evidence in favor of  $M_1$  models. Legend: bold, 0-0.5, 'barely worth mentioning'; gray striped, 0.5-1, 'positive evidence'; dark-gray striped, 1-2, 'strong evidence'.

576 Summarizing, we can say that the evidence in favor of  $\mathbf{R}_E$  is sufficiently significant  
577 in MR<sub>1</sub> and MR<sub>3</sub>, whereas in the other MRs,  $\mathbf{R}_S$  performs just slightly better than  
578 the other models; anyhow, in all of the MRs the information on the faulting geometry  
579 provided through the rupture area (A) appears to improve the performance of the SR  
580 model. Note that MR<sub>1</sub> has only seven events associated with two fault sources and a  
581 poorly constrained tectonic setting; therefore, the results of this MR must be considered

582 with caution. With reference to Equations (8-11), recalling that the rupture area is  
583 obtained by the regression  $\log_{10} A_w = a + b M_w$  with  $b \in \{0.82, 0.90, 0.98\}$  according  
584 to the faulting type (Wells & Coppersmith, 1994), it turns out that  $X_B \propto 10^{0.75 M_s}$ ,  
585  $X_M \propto 10^{1.5 M_w}$ ,  $X_E \propto 10^{(1.76, 1.84) M_w}$ , and  $X_S \propto 10^{(0.26, 0.34) M_w}$ , where  $(.,.)$  indicates the  
586 variability range of the magnitude coefficient. The same order of size of this coefficient  
587 in  $\mathbf{R}_B$ - $\mathbf{R}_S$  and  $\mathbf{R}_M$ - $\mathbf{R}_E$  can explain the similar performances of these models in the MRs  
588 where no or few events with  $M_w \geq 6.5$  were recorded.

### 589 5.2.2 Retrospective forecast validation

590 Another tool to compare the performances of the four versions of the SR model is the  
591 analysis of their forecasting skill through retrospective forecast validation. Table 8 shows  
592 the value of the Ando & Tsay information criterion (Eq. (21)) for each model and for  
593 each MR. In the seven MRs of MR<sub>2</sub>-MR<sub>8</sub>, the highest value is given by model  $\mathbf{R}_S$ , and in  
594 the remaining MR<sub>1</sub>, by model  $\mathbf{R}_E$ . These results agree with those provided by the Bayes  
595 factor, except for MR<sub>3</sub> where, however, the values are very similar. In all of the cases  
596 except MR<sub>1</sub>, as the pairwise differences are less than 2, there is slight evidence in favor of  
597 these models.

model region	$R_B$	$R_M$	$R_E$	$R_S$
MR <sub>1</sub>	70.7222	64.6214	<b>63.4842</b>	73.5678
MR <sub>2</sub>	127.5156	128.6673	128.6785	<b>126.1706</b>
MR <sub>3</sub>	226.8038	227.2734	227.3653	<b>226.5803</b>
MR <sub>4</sub>	233.6563	234.7216	234.8703	<b>231.9754</b>
MR <sub>5</sub>	102.7009	103.3292	103.4852	<b>100.2118</b>
MR <sub>6</sub>	131.4636	131.4883	131.2725	<b>130.4955</b>
MR <sub>7</sub>	200.3160	200.3123	200.1481	<b>199.6899</b>
MR <sub>8</sub>	164.4944	164.6212	164.5529	<b>162.4373</b>

Table 8: Ando & Tsay information criterion (Eq. (21) times  $-2n$ ) evaluated for the four stress release models. Bold: minimum value, which indicates the best model in each MR.

598 Another retrospective validation is carried out by evaluating the expected occurrence

599 time of each earthquake (target event) included in each MR dataset, from right after the  
 600 occurrence of the event that precedes it. The discrepancies between the expected times  
 601 and the actual earthquake occurrence times can then be calculated. To this end, we use  
 602 the Gompertz distribution (Equation 32) and its statistical summaries: mean, median,  
 603 75% HPD interval, and 90% HPD interval. Figure 7 provides two forecast examples: one,  
 604 (retrospectively) issued for MR<sub>1</sub> on 1854/12/29, the date of the occurrence of a  $M_w$  5.77  
 605 earthquake, shows a waiting time to the next event that relatively closely predicts the  
 606 occurrence date of the 1887/02/23,  $M_w$  6.29, earthquake; the other is issued for MR<sub>2</sub> on  
 607 1776/07/10, the date of occurrence of a  $M_w$  5.82 earthquake, and closely predicts the  
 608 waiting time to the 1788/10/20,  $M_w$  5.71, earthquake. Note the different shapes of the  
 609 two density functions that characterize the expected interevent times that vary from more  
 610 than 30 years to about 12 years.

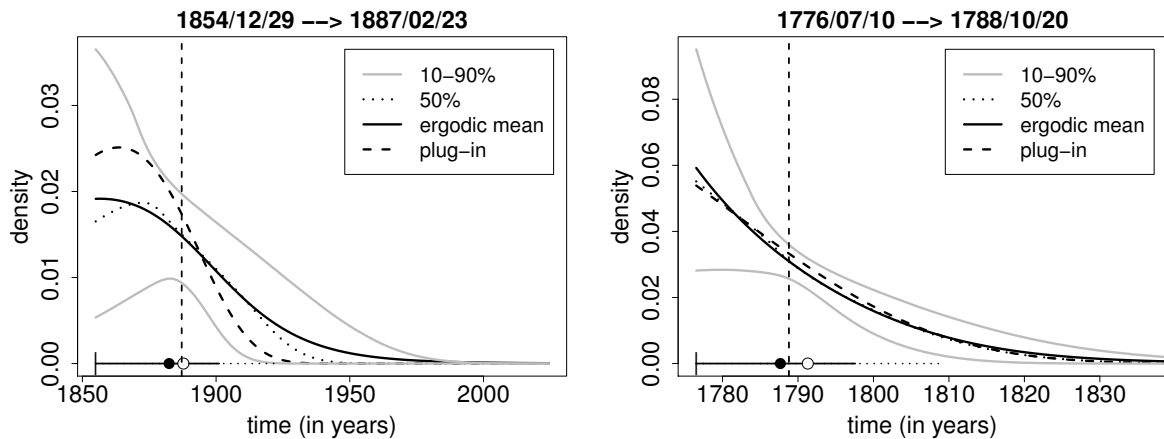


Figure 7: Examples of the estimated density functions of the time to next event, and their statistical summaries. Legend: Gompertz density function (solid curve), mean (open circle), median (solid circle), and 75% HPD (solid horizontal segment) and 90% HPD (dotted horizontal segment) intervals. The forecast issue date is denoted by a short vertical bar ( $|$ ), and the occurrence time of the target event by a long, dashed, vertical line. The examples are taken from MR<sub>1</sub> (left) and MR<sub>2</sub> (right) and are based on the  $\mathbf{R}_E$  and  $\mathbf{R}_S$  models, respectively.

611 Table 9 summarizes the discrepancies of the forecasts for the four versions of the SR

612 model for the eight MRs, in terms of the average lengths of the 75% HPD and 90% HPD  
613 intervals, as well as the mean absolute (root-mean-square) errors between the medians  
614 (means) and the observed times. For the absolute error, it is reasonable to compute its  
615 standard deviation, which is of the same order of magnitude as its mean in all of the  
616 MRs. In all of the MRs, the lowest values (or minimum discrepancy) essentially confirm  
617 the models chosen according to the Bayes factor (Table 7), except for MR<sub>3</sub>; in this MR,  
618 even if the values of the indicators are very similar to each other, they support the model  
619  $R_S$  in agreement with the Ando & Tsay information criterion (see Table 8). Hence,  
620 hereinafter we report the results provided by model  $\mathbf{R_E}$  for MR<sub>1</sub>, and by model  $\mathbf{R_S}$  for  
621 the remaining MRs. The energy and the scaled energy again appear to be the appropriate  
622 quantities to be used in SR models.

Region	Model	HPD average length		Average discrepancy	
		90%	75%	Median	Mean
MR <sub>1</sub>	$R_B$	94.4	65.9	27.9	40.7
	$R_M$	64.6	44.4	14.4	26.4
	$R_E$	<b>62.5</b>	<b>42.8</b>	<b>13.8</b>	<b>25.3</b>
	$R_S$	117.8	78.1	37.6	51.0
MR <sub>2</sub>	$R_B$	33.8	<b>20.8</b>	9.1	12.6
	$R_M$	35.2	21.1	9.3	13.2
	$R_E$	35.3	21.0	9.2	13.1
	$R_S$	<b>31.8</b>	<b>20.8</b>	<b>8.8</b>	<b>11.7</b>
MR <sub>3</sub>	$R_B$	14.0	<b>8.4</b>	<b>4.6</b>	<b>7.4</b>
	$R_M$	14.1	8.5	<b>4.6</b>	7.5
	$R_E$	14.1	8.5	4.7	7.5
	$R_S$	<b>13.9</b>	<b>8.4</b>	<b>4.6</b>	<b>7.4</b>
MR <sub>4</sub>	$R_B$	19.9	12.0	<b>6.6</b>	8.8
	$R_M$	20.0	<b>11.9</b>	6.7	9.1
	$R_E$	20.0	<b>11.9</b>	6.7	9.1
	$R_S$	<b>19.3</b>	12.1	<b>6.6</b>	<b>8.6</b>
MR <sub>5</sub>	$R_B$	31.1	19.3	8.7	12.1
	$R_M$	32.0	<b>19.0</b>	8.7	12.6
	$R_E$	32.1	<b>19.0</b>	8.8	12.7
	$R_S$	<b>27.8</b>	19.2	<b>8.1</b>	<b>10.7</b>
MR <sub>6</sub>	$R_B$	50.5	32.4	12.8	17.7
	$R_M$	51.6	32.7	13.2	18.0
	$R_E$	51.9	33.1	13.2	18.1
	$R_S$	<b>48.1</b>	<b>32.3</b>	<b>12.2</b>	<b>17.0</b>
MR <sub>7</sub>	$R_B$	21.1	12.6	6.9	8.5
	$R_M$	21.1	12.6	6.9	8.5
	$R_E$	21.0	<b>12.5</b>	6.9	8.5
	$R_S$	<b>20.8</b>	12.6	<b>6.8</b>	<b>8.3</b>
MR <sub>8</sub>	$R_B$	50.6	30.4	14.6	19.9
	$R_M$	51.2	30.5	14.7	20.2
	$R_E$	51.1	30.5	14.7	20.1
	$R_S$	<b>46.4</b>	<b>30.1</b>	<b>14.2</b>	<b>18.3</b>

Table 9: Ability of retrospective forecasting of the four stress release models in each MR, in terms of the following indicators: average length of the 75% and 90% HPD intervals, the mean absolute (root-mean-square) error between the expected median (mean) and observed occurrence times. Bold, lowest values.

623 Figure 8 shows the results of the retrospective validation of all of the data in MR<sub>3</sub> by  
624 representation of the statistical summaries of the estimated Gompertz density functions  
625 (see examples in Figure 7). The results for the other MRs are shown in Appendix C  
626 (Figures C1-C7). In these figures the reliability of the forecasts is expressed as the time  
627 discrepancy with respect to the actual occurrence of the targeted event. As a visual  
628 tip, for comparing the various discrepancies one with the other, time lines are vertically

629 aligned with respect to the actual occurrence time of the target events. Forecasts to the  
630 right of the alignment thus correspond to overestimations of the interevent time, and the  
631 opposite for those to the left. In the case of  $MR_3$ , the actual event time is outside the  
632 90% HPD interval only for 4 of the 39 events examined, whereas for 30 events it is within  
633 the 75% HPD interval.

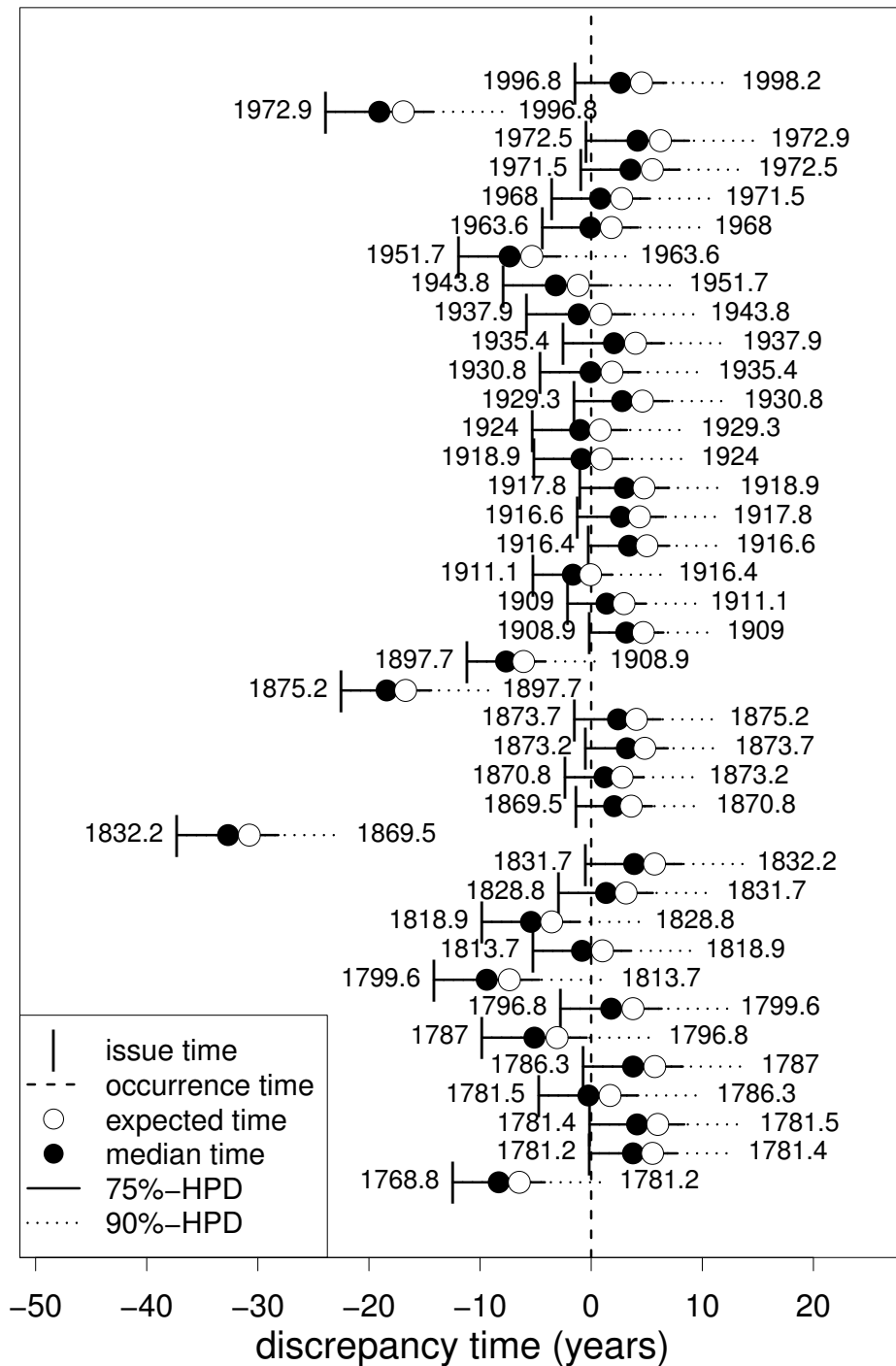


Figure 8: Time lines of 39 retrospective forecasts for  $MR_3, R_S$  model, in order of descending date from the top to the bottom. Each forecast is as would have been issued on the occurrence date (shown on the left, and marked by a short vertical bar) of an event in the MR dataset, and is aimed at predicting the date (on the right) of the next event (target). The forecasts are shown by the statistical summaries of their Gompertz density functions (see Figure 7). The time lines are shifted laterally so that they intersect the vertical dashed line at the actual occurrence<sup>39</sup> date of the target event.

### 634 5.2.3 Prospective forecast validation

635 To conduct prospective validation, there is the need to first determine which earthquakes  
636 that occurred since the beginning of 2003 are consistent with the learning dataset used.  
637 To this end, we used CPTI11 for the period from 2003-2006, and ISIDe for the period  
638 from 2007-2012 (see Section 3), where there were the following four earthquakes:

- 639 1. 2003/09/14,  $M_w = 5.29 \pm 0.09$  (from CPTI11), Bolognese Apennines, reverse  
640 faulting, MR<sub>3</sub>;
- 641 2. 2008/12/23,  $M_w = 5.4$ , ( $M_l = 5.2$ , from ISIDe), Parma, reverse faulting, MR<sub>3</sub>;
- 642 3. 2012/05/20,  $M_w = 5.9$  ( $M_l = 5.9$ , from ISIDe), Finale Emilia, reverse faulting,  
643 MR<sub>3</sub>;
- 644 4. 2009/04/06,  $M_w = 6.1$  ( $M_l = 5.9$ , from ISIDe), L'Aquila, MR<sub>4</sub>.

645 The CPTI11 catalog assigns earthquake #1 a magnitude that is very close to the  
646 threshold ( $M_w \geq 5.3$ ) that we considered for the learning phase. However, Rovida et  
647 al. (2011) reported that the use of new empirical relations in CPTI11 decreases the  
648 magnitudes  $< 5.5$  and increases those  $> 5.5$ , with respect to the CPTI04. Therefore,  
649 according to the rules of our learning catalog (CPTI04), the 2003/09/14 earthquake would  
650 be likely to be beyond the threshold, and we thus include it in the validation procedure  
651 with  $M_w = 5.3$ . The three earthquakes with  $M_w \geq 5.3$  that occurred in the period 2007-  
652 2012 (#2, #3, and #4) are taken from ISIDe by exclusion of their aftershocks, i.e., for  
653 homogeneity with the CPTI04 declustering, the events that occurred within 30 km and 90  
654 days are excluded. Note also that ISIDe uses local magnitude ( $M_l$ ), and thus we obtain  
655  $M_w$  values using the same conversion formula ( $M_w = 0.812 M_l + 1.145$ ) used for the  
656 compilation of CPTI04 (MPS Working Group 2004 , 2004).

657 The various magnitude determinations for earthquake #4 span a wide range that  
658 depends on the co-existence of source and path complexities and heterogeneities in the  
659 local seismic response (Ameri et al. , 2012). The most significant magnitude values are:  
660  $M_l = 5.9$ , based on the INGV seismic bulletin from ISIDe;  $M_w = 6.08$ , based on the time-  
661 domain moment tensor (Scognamiglio et al. , 2010);  $M_w = 6.13$ , based on the regional



662 moment tensor (Herrmann et al. , 2011);  $M_l = 6.08 \pm 0.17$ , based on the Huber mean  
663 of accelerometric determinations (Maercklin et al. , 2011); and  $M_w = 6.3$ , based on the  
664 regional centroid moment tensor (Pondrelli et al. , 2010). We thus adopt  $M_w = 6.1$ , as  
665 this appears to be the most frequent value.

666 Table 10 summarizes the prospective forecasts provided by the  $\mathbf{R}_E$  model for MR<sub>1</sub>,  
667 and by the  $\mathbf{R}_S$  model for the other MRs. Note that the forecast issue dates considered  
668 here are: the date of the latest event in each MR learning dataset; the end date of the  
669 learning catalog (end of 2002, everywhere); the date when any earthquake occurred in  
670 each MR over the years 2003-2012 (in our case in MR<sub>3</sub> and MR<sub>4</sub>); and the beginning of  
671 2013. Forecasts are addressed in terms of the probability distribution of the time to the  
672 next event, as summarized by the median, the mean, and its standard deviation, as well  
673 as by the 75% HPD and 90% HPD intervals.

674 In MR<sub>4</sub>, after the last observed event in the learning catalog (2001/11/26; Table 10,  
675 first line in the MR<sub>4</sub> block), it can be expected that the next earthquake with  $M_w \geq 5.3$   
676 will be in early 2011 according to the mean, with a standard deviation of  $\pm 8.4$  years; or by  
677 2008.4, 2014.7, or 2022.7 with probabilities of 50%, 75%, and 90%, respectively. A little  
678 more than a year later (2003/01/01; Table 10, second line), by adding the information  
679 that no event had occurred in the meanwhile, the expected time to the next event moves  
680 forward by a year. This additional information not only lengthens the waiting time to  
681 the next event, but also reduces the uncertainty on the HPD interval length. After the  
682 2009/04/06 earthquake (Table 10, third line), the estimation of the model parameters is  
683 fully repeated when the new earthquake is added to the dataset. Based on the seismic  
684 and tectonic knowledge available in 2002, and reinforced only with the addition of about  
685 10 years of seismic history (Table 10, fourth line), the  $\mathbf{R}_S$  model predicts that the next  
686 earthquake with  $M_w \geq 5.3$  in MR<sub>4</sub> can be expected in 2022, according to the mean value,  
687 or by 2019.5, 2025.8, and 2033.7, with probabilities of 50%, 75%, and 90%, respectively.

Region	Date of forecast issue	HPD 75%	HPD 90%	Median	Mean (st.dev.)
MR <sub>1</sub>	1887.2	2046.6-2327.3	1985.7-2401.5	2190.8	2198.1 (54.5)
	2003.0	2040.9-2304.0	2003.0-2359.0	2191.7	2204.2 (48.9)
	2013.0	2044.4-2301.0	2013.0-2360.1	2193.9	2207.3 (48.3)
MR <sub>2</sub>	1977.7	1977.7-2009.8	1977.7-2025.9	1994.9	1999.9 (16.9)
	2003.0	2003.0-2024.0	2003.0-2036.9	2013.8	2018.1 (13.4)
	2013.0	2013.0-2033.0	2013.0-2045.9	2023.2	2027.7 (13.4)
MR <sub>3</sub>	1998.2	1998.2-2006.7	1998.2-2012.5	2002.4	2004.4 ( 6.1)
	2003.0	2003.0-2011.1	2003.0-2016.7	2007.0	2008.9 ( 5.9)
	2003.7 <sup>(a)</sup>	2003.7-2011.6	2003.7-2016.9	2007.6	2009.4 ( 5.7)
	2009.0 <sup>(b)</sup>	2009.0-2016.8	2009.0-2022.1	2012.8	2014.7 ( 5.6)
	2012.4 <sup>(c)</sup>	2012.4-2020.2	2012.4-2025.5	2016.3	2018.1 ( 5.6)
	2013.0	2013.0-2020.8	2013.0-2026.2	2016.9	2018.7 ( 5.6)
MR <sub>4</sub>	2001.9	2001.9-2014.7	2001.9-2022.7	2008.4	2011.0 ( 8.4)
	2003.0	2003.0-2015.6	2003.0-2023.5	2009.4	2012.0 ( 8.3)
	2009.3 <sup>(d)</sup>	2009.3-2022.3	2009.3-2030.4	2015.9	2018.5 ( 8.5)
	2013.0	2013.0-2025.8	2013.0-2033.7	2019.5	2022.1 ( 8.3)
MR <sub>5</sub>	2002.8	2002.8-2019.2	2002.8-2029.5	2011.5	2015.0 (11.1)
	2003.0	2003.0-2019.3	2003.0-2029.6	2011.6	2015.2 (11.1)
	2013.0	2013.0-2028.4	2013.0-2039.9	2020.7	2024.8 (11.8)
MR <sub>6</sub>	1998.7	1998.7-2029.0	1998.7-2047.3	2014.7	2020.8 (19.7)
	2003.0	2003.0-2031.7	2003.0-2049.6	2018.0	2024.1 (19.2)
	2013.0	2013.0-2040.5	2013.0-2059.0	2027.0	2033.5 (19.4)
MR <sub>7</sub>	2001.4	2001.4-2012.5	2001.4-2020.4	2006.8	2009.6 ( 8.4)
	2003.0	2003.0-2014.0	2003.0-2021.9	2008.4	2011.1 ( 8.3)
	2013.0	2013.0-2025.0	2013.0-2033.7	2018.9	2021.9 ( 9.1)
MR <sub>8</sub>	2002.7	2002.7-2035.0	2002.7-2053.8	2019.4	2025.5 (19.5)
	2003.0	2003.0-2035.3	2003.0-2054.0	2019.7	2025.7 (19.5)
	2013.0	2013.0-2043.9	2013.0-2061.9	2029.1	2035.0 (19.1)

- (a) just after 2003/09/14 earthquake,  $M_w$  5.3  
(b) just after 2008/12/23 earthquake,  $M_w$  5.4  
(c) just after 2012/05/20 earthquake,  $M_w$  5.9  
(d) just after 2009/04/06 earthquake,  $M_w$  6.1

Table 10: Prospective forecasts according to the  $R_E$  model in MR<sub>1</sub>, and to the  $R_S$  model in the other MRs. All of the dates are expressed in decimal years. The estimated probability distribution of the time to the next event is expressed as: 75% and 90% HPD intervals, median, mean, and standard deviation (years).

688 In MR<sub>3</sub>, three earthquakes occurred in the period 2003-2012, and thus the forecasts can  
689 be successively updated after each one of these. Note that all of these successive forecasts  
690 fall within the 75% HPD interval, and that the average absolute error of the forecast time  
691 for all three of these occurrences is 1.7 years when considering the median values, whereas  
692 the root-mean-square error is 3.29 years when considering the mean values.

693 We note that the model parameters are fully re-estimated after every new earthquake,  
694 by its inclusion in the learning dataset of the MR. The robustness of these parameter  
695 estimates is shown by the similar intensity functions (Figure 9) they allow, and the similar

696 values they achieve (Table B1).

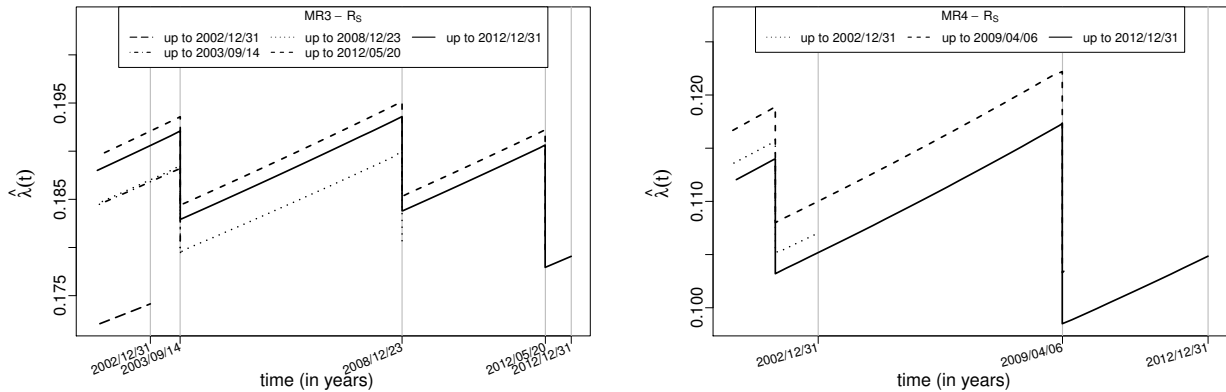


Figure 9: Estimate (ergodic mean) of the intensity function for the  $\mathbf{R}_S$  model in  $\text{MR}_3$  and  $\text{MR}_4$ , updated whenever new information (i.e., earthquake occurrence) is included in the relevant dataset.

697 For completeness of information, Table C1 provides a summary of all of the forecasts  
 698 issued at the end of the learning catalog (end of 2002) for the four versions of the SR  
 699 model for each MR.

### 700 5.3 Comparison with the Poisson model

701 The Poisson model is a time-independent point process that is defined by its conditional  
 702 intensity function  $\lambda(t) = e^\alpha$ , where  $\alpha$  is a real parameter; in particular, a SR model where  
 703 the  $b$  parameter tends to zero is a Poisson model. In this view, it is apparent that the SR  
 704 model is conceived as a time-dependent version of the Poisson model, and its conditional  
 705 intensity function is expected to evolve in time around an average rate according to the  
 706 variation of the level of ‘stress’ in the region. To compare the performances of the Poisson  
 707 and SR models, the results on the Bayesian analysis of the Poisson model for each MR  
 708 are summarized below. Similar to the results in Table 5, the Poisson parameter  $\alpha$  is  
 709 estimated for each MR; from  $\text{MR}_1$  to  $\text{MR}_8$  respectively, these estimates are  $-4.11$ ,  $-2.67$ ,  
 710  $-1.78$ ,  $-2.12$ ,  $-2.51$ ,  $-3.05$ ,  $-2.16$ , and  $-3.03$ . Similar to Tables 6 and 7, Table 11 shows  
 711 the estimated values of the marginal  $\log_{10}$  likelihoods and the Bayes factors between the  
 712 versions of the SR and Poisson models.

713 For the marginal  $\log_{10}$  likelihood, the Poisson model behaves worse than the best SR  
714 model for each MR. Based on the Bayes factor, we can note: positive/ strong evidence  
715 in favor of model  $R_E$  in MR<sub>1</sub> and MR<sub>3</sub>; on the whole, positive/ strong evidence in favor  
716 of the SR models in MR<sub>4</sub>, MR<sub>7</sub>, and MR<sub>8</sub>; and slight evidence in favor of  $R_S$  in the  
717 remaining MRs.

Region	marg. $\log_{10} \mathcal{L}$	$\log_{10} B_{12}$			
		$R_B$	$R_M$	$R_E$	$R_S$
MR <sub>1</sub>	-15.8748	<b>0.7279</b>	<b>2.0063</b>	<b>2.2791</b>	<b>0.2168</b>
MR <sub>2</sub>	-27.3635	<b>0.0262</b>	-0.2294	-0.2052	<b>0.2392</b>
MR <sub>3</sub>	-49.7749	<b>0.0800</b>	-0.0207	<b>0.7866</b>	<b>0.0405</b>
MR <sub>4</sub>	-52.3692	<b>1.9704</b>	<b>1.7573</b>	<b>1.7374</b>	<b>2.2144</b>
MR <sub>5</sub>	-21.7897	-0.1705	-0.2864	-0.3353	<b>0.2971</b>
MR <sub>6</sub>	-28.5106	<b>0.2513</b>	<b>0.2531</b>	<b>0.2897</b>	<b>0.4080</b>
MR <sub>7</sub>	-43.7551	<b>0.6019</b>	<b>0.6080</b>	<b>0.6622</b>	<b>0.7377</b>
MR <sub>8</sub>	-36.1995	<b>0.8118</b>	<b>0.7712</b>	<b>0.8507</b>	<b>1.1933</b>

Table 11: Global summary measures of the performance of the Poisson model in each MR: (marg. $\log_{10} \mathcal{L}$ ), marginal  $\log_{10}$  likelihood; ( $\log_{10} B_{12}$ ), logarithm of the Bayes factors of the four SR models,  $M_1$ , versus Poisson model,  $M_2$ . As for the Bayes factor, the Jeffreys' scale is used for rating the evidence in favor of  $M_1$  models: bold, 0-0.5, 'barely worth mentioning'; gray striped, 0.5-1, 'positive evidence'; dark-gray striped, 1-2, 'strong evidence'.

718 Table 12 shows the results of the retrospective forecast validation by applying the  
719 Poisson model to each MR. We recall that according to the Poisson model, the waiting  
720 time to the next event is exponentially distributed with mean  $e^{-\alpha}$ , and consequently the  
721 forecast is time-independent. By comparing this with the results in Table 9, we note  
722 that the 90%-HPD intervals and all of the average discrepancies between the observed  
723 occurrence times and the forecasted values estimated by the best SR model are less than  
724 those of the Poisson model, whereas the 75%-HPD intervals related to the Poisson model  
725 are narrower.

726 Taking the cue from this slightly larger uncertainty of the forecasts issued by the SR  
727 model, we highlight that the values in Table 9 are computed immediately after an event

728 and that they can be updated as time passes and no occurrence happens, obtaining a  
729 reduction in the 75% and 90% HPD intervals of the waiting time variable (as shown in  
730 Table C1); of course this is not possible with the homogeneous Poisson model, for which  
731 the mean and variance of the waiting time do not depend on the time elapsed since the  
732 last event. This is more clearly depicted in Figure 10; through the model  $R_S$ , we calculate  
733 the forecasts issued immediately, and 10, 20 and 30 years since the 1922/12/29 earthquake  
734 in MR<sub>4</sub>. We note that the forecasts are modified based on the additional information on  
735 nonoccurrence, and that the average waiting times and HPD intervals are shortened.

Region	HPD length		Average discrepancy	
	90%	75%	Median	Mean
MR <sub>1</sub>	154.1	87.1	41.9	61.7
MR <sub>2</sub>	34.5	<b>20.2</b>	9.1	12.4
MR <sub>3</sub>	<b>13.9</b>	<b>8.3</b>	4.8	7.6
MR <sub>4</sub>	19.6	<b>11.7</b>	6.7	9.2
MR <sub>5</sub>	29.7	<b>17.3</b>	8.3	12.3
MR <sub>6</sub>	50.8	<b>29.8</b>	14.4	20.2
MR <sub>7</sub>	<b>20.4</b>	<b>12.1</b>	<b>6.8</b>	8.5
MR <sub>8</sub>	49.1	<b>29.0</b>	14.7	20.3

Table 12: Ability of retrospective forecasting of the Poisson model in each MR, in terms of the following indicators: length of the 75% and 90% HPD intervals, and mean absolute (root-mean-square) error between the expected median (mean) and the observed occurrence times. Bold, the lowest values for each MR compared to those in Table 9.

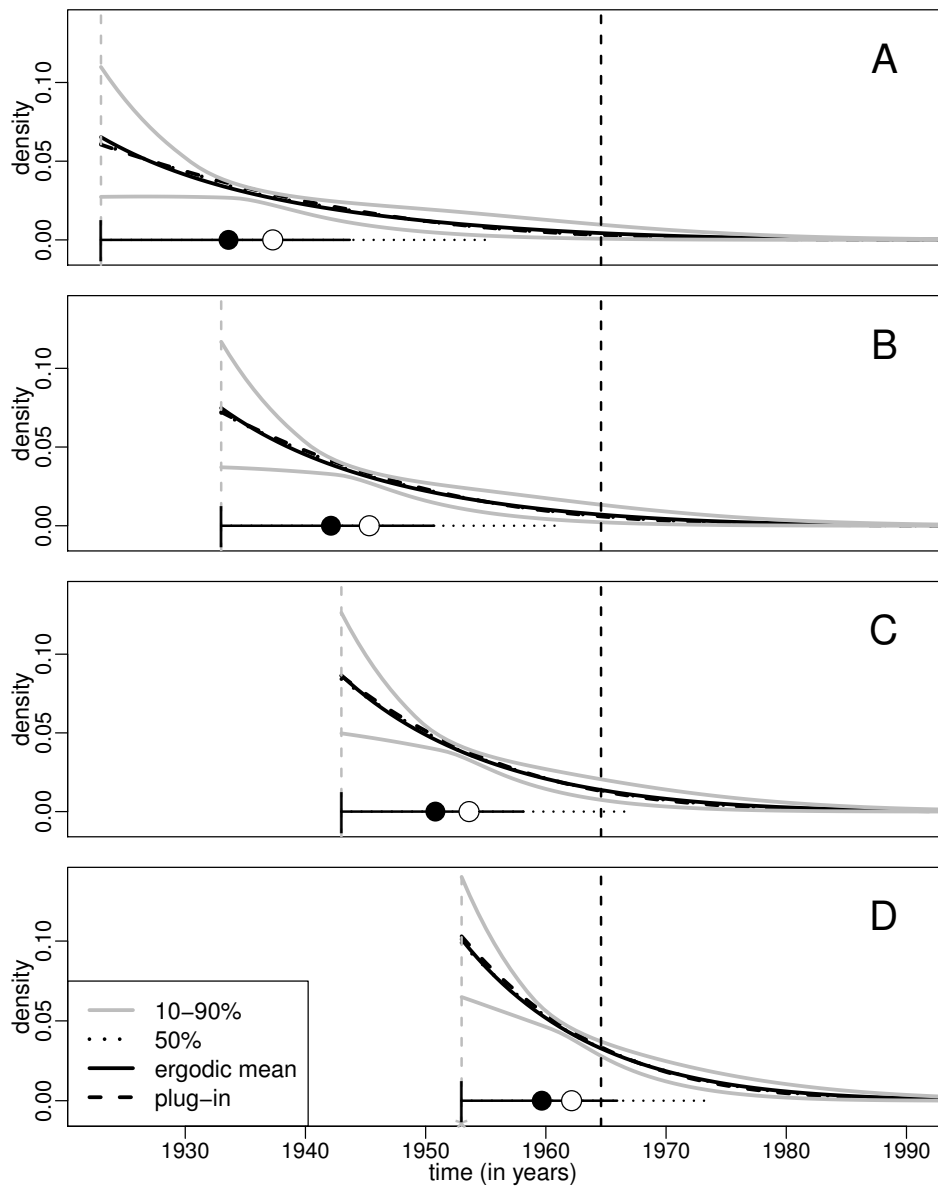


Figure 10: Density functions of the time to the next event and their statistical summaries, estimated at different issue times before the 1964/08/02 earthquake in  $MR_4$  according to model  $\mathbf{R}_S$ . The forecast issue dates are for immediately after the 1922/12/29 earthquake (A), and for 10 years (B), 20 years (C), and 30 years (D) after this event. Legend: Gompertz density function (solid curve), mean (open circle), median (solid circle), 75% HPD (solid horizontal segment), and 90% HPD (dotted horizontal segment). The forecast issue date is indicated by the gray dashed vertical line, and the occurrence time of the target event by the black dashed vertical line.

## 6 Final remarks

We examined four different versions of the classic SR model, based on the probabilistic translation of the elastic rebound theory and including the contribution of the tectonic information. All of these model versions imply a sudden hazard reduction right after a strong earthquake (threshold set at  $M_w \geq 5.3$ ) and an exponentially increasing hazard function between two consecutive earthquakes (excluding the aftershock sequences).

The four model versions, however, differ from one to the other in the quantity - strain, moment, energy, and scaled energy - as chosen to represent the physical process responsible for the generation of earthquakes. Equations (8)-(11) highlight the key elements (i.e., earthquake magnitude, fault rupture area, exponential coefficient) that quantify the abrupt change in the system when an earthquake occurs. The affinity among these elements is reflected in the similarity of the shapes of the relevant conditional intensities (Figures 5 and 6). Despite the general similarity, note that the conditional intensity variation (equivalent to a hazard drop) is different in the different SR models, depending on the sizes of the intervening earthquake. With reference to Figure 6, take for example the amount of the vertical drop in the conditional intensity after the 1915/01/13,  $M_w = 6.99$ , earthquake and the vertical drop after all of the other moderate earthquakes ( $M_w < 6$ ). The ratio between these two values for the  $\mathbf{R}_S$  model is much smaller than the same ratio in any of the  $\mathbf{R}_B$ ,  $\mathbf{R}_M$ , and  $\mathbf{R}_E$  models. In other words, when the scaled energy is adopted, the SR model produces a hazard decrease that is relatively heightened for smaller earthquakes and abated for larger earthquakes.

As for the model comparisons, the Bayes factor indicates (Table 7) that the  $\mathbf{R}_S$  model performs, slightly in  $MR_2$ ,  $MR_4$ ,  $MR_6$ - $MR_8$ , and moderately, in  $MR_5$ , better than the other models.  $\mathbf{R}_E$  performs considerably better than the others in  $MR_1$  and moderately so in  $MR_3$ . However, we note that the results for  $MR_1$  should be taken cautiously because of the lower number of events (only seven) and its nonuniform tectonic characterization. For the predictive performance, the Ando & Tsay information criterion supports (Table 8) the conclusions reached by the Bayes factor, except for  $MR_3$ , where the criterion assigns slight evidence in favor of  $\mathbf{R}_S$ . Overall, although the differences among the model performances

765 are not clearly significant, we suggest that adopting the energy or the scaled energy as a  
766 proxy measure of earthquake size is advisable. Indeed, the scaled energy allows the model  
767 to be enhanced with information on the rupture parameters, such as the area and the  
768 mechanism, which can be expected to become progressively less uncertain, in the future,  
769 as knowledge of earthquake faulting improves (e.g., fault scaling relationships).

770 The probability distribution of the time to next event for the SR model has been ana-  
771 lytically identified as the Gompertz distribution (Section 4.2.3) with two parameters that  
772 depend on the model parameters and on the value of the hazard function at time  $t$  (Section  
773 4.2.3). After summarizing its main properties, we examined the Gompertz distribution  
774 in the Bayesian framework by evaluation of its posterior predictive distribution through  
775 the Markov chains generated from the posterior distributions of the model parameters in  
776 the estimation procedure (the MCMC algorithm is detailed in Appendix B). These find-  
777 ings bring about immediate benefit, by allowing modelers to avoid approximating this  
778 distribution through numerical simulations (e.g., Wang et al. 1991). We thus used  
779 the Gompertz distribution and its statistical summaries to run a set of retrospective and  
780 prospective forecasts of the occurrence times of the main shocks, and then we validated  
781 the procedure against the data observed.

782 Retrospective forecasts have also been used as a further criterion for supporting the  
783 selection of the best SR models. Different measures of the discrepancy between the  
784 expected occurrence time of an earthquake and the time of its actual occurrence (Table  
785 9) have shown that the retrospective analysis supports the choice of the  $\mathbf{R}_S$  model in most  
786 of the cases analyzed here.

787 Based on the knowledge available in 2002 in terms of the seismicity and tectonics,  
788 prospective forecasts issued at the very beginning of 2003 indicated that in decreasing  
789 order of immediacy, MR<sub>3</sub>, MR<sub>7</sub>, and MR<sub>4</sub> were the most prone areas to be hit by earth-  
790 quakes of  $M_w \geq 5.3$  in the following decade (Table 10). Of these MRs, earthquakes have  
791 actually occurred in MR<sub>3</sub> (three events) and MR<sub>4</sub> (one event) with forecasts in terms of  
792 median and mean with an average accuracy of about 6 years. However, no earthquake has  
793 occurred in MR<sub>7</sub> up to the end of 2012. By adding this information to the 2013 update,



794 the forecast postpones the expected occurrence time of the next event considerably (by  
795 more than 10 years).

796 As we anticipated in Section 4.2.3, updating a forecast during the waiting time by  
797 adding the information that no earthquake has occurred tends to postpone the time to  
798 the next event and to reduce the uncertainty around that value. This effect is achieved  
799 through the shortening and peaking of the probability density function of the time to the  
800 next event. The prospective forecasts reported in Table 10 confirm this general behav-  
801 ior, although the amount of delay and uncertainty gain remain variable, and depend on  
802 repeated parameter estimates.

803 It is important to recall that both the time and space scales of the SR models and their  
804 associated uncertainties that we have investigated here depend on the characteristics of  
805 the available datasets. Note that there is a trade-off between the size of the region to be  
806 investigated and the length of the learning dataset. On the one hand, a reduction in the  
807 size of the region would be likely to improve its tectonic characterization, which would  
808 allow the analyst to single out homogeneous faults and avoid mixing tectonic structures  
809 that obey mechanically different stress-loading systems. It would also imply a smaller  
810 spatial domain within which the forecasted earthquakes can occur. On the other hand, a  
811 smaller area would capture fewer earthquakes for building the learning dataset, thereby  
812 worsening the robustness and overall quality of the SR model. The balancing of these  
813 factors (tectonics and seismicity) in the Italian case allowed us to investigate only a limited  
814 number of cases (the eight MRs). Additional studies are thus needed for the exploration  
815 of more fault systems with different seismic histories, to further test the energy and scaled  
816 energy as the best option in SR models, and for the refining of the time-space limits of the  
817 SR model applications in robust earthquake forecasting. Similar limitations hold for the  
818 application of the interesting extension of the SR model which was presented by Jiang et  
819 al. (2011) and which requires knowledge of source parameters that are rarely available  
820 for historical Italian earthquakes.

821 Depending on the data availability, possible future research directions can also be  
822 aimed at developing the *linked* (or *coupled*) versions of the SR models (e.g., Bebbington

823 & Harte 2003, Kuehn et al. 2008) on the same Italian data, using the (scaled) energy  
824 as the measure of the sizes of the events.

## 825 **Acknowledgements**

826 We are grateful to two reviewers for their helpful comments. The authors also thank  
827 Fracassi and Valensise for providing the earthquake association with fault sources. This  
828 study was partially funded by the Italian Dipartimento della Protezione Civile in the  
829 framework of the 2007-2009 Agreement with Istituto Nazionale di Geofisica e Vulcanologia  
830 (INGV), project S1: “Analysis of the seismic potential in Italy for the evaluation of the  
831 seismic hazard”.

## 832 **References**

- 833 Abramowitz, M. & Stegun, I.A., 1972. *Handbook of Mathematical Functions*, Dover Pub-  
834 lications, New York.
- 835 Ameri, G., Gallovic, F. & Pacor, F., 2012. Complexity of the Mw 6.3 2009 L’Aquila  
836 (central Italy) earthquake: 2. Broadband strong motion modeling, *J. Geophys. Res.:  
837 Solid Earth*, **117**, B04308, doi:10.1029/2011JB008729.
- 838 Ando, T. & Tsay, R., 2010. Predictive likelihood for Bayesian model selection and aver-  
839 aging, *International Journal of Forecasting*, **26**, 744-763.
- 840 Basili, R., Valensise, G., Vannoli, P., Burrato, P., Fracassi, U., Mariano, S., Tiberti, M.M.  
841 & Boschi, E., 2008. The Database of Individual Seismogenic Sources (DISS), version 3:  
842 summarizing 20 years of research on Italy’s earthquake geology, *Tectonophysics*, **453**,  
843 1-4, 20-43, doi: 10.1016/j.tecto.2007.04.014
- 844 Basili, R., Kastelic, V., Valensise, G. & DISS Working Group 2009, 2009. DISS3  
845 tutorial series. Guidelines for Compiling Records of the Database of Indi-  
846 vidual Seismogenic Sources, Version 3, *Rapporti Tecnici INGV 108*, 20 pps.,

847 <http://portale.ingv.it/produzione-scientifica/rapporti-tecnici-ingv/archivio/rapporti->  
848 [tecnici-2009/](http://portale.ingv.it/produzione-scientifica/rapporti-tecnici-ingv/archivio/rapporti-tecnici-2009/)

849 Bebbington, M. & Harte, D.S., 2003. The linked stress release model for spatio-temporal  
850 seismicity: formulations, procedures and applications, *Geophys. J. Int.*, **154**, 3, 925-946.

851 Benioff, H., 1951. Earthquakes and rock creep, Part I: Creep characteristics of rocks and  
852 the origin of aftershocks, *Bull. Seism. Soc. Am.*, 41, 31-62.

853 Berger, J., 2006. The case for objective Bayesian analysis, *Bayesian Anal.*, **1**, 3, 385-402.

854 Bhattacharyya, P. & Chakrabarti, B.K. et al., 2006. *Modelling Critical and Catastrophic*  
855 *Phenomena in Geoscience*, Lect. Notes Phys., 705, Springer, Berlin Heidelberg, DOI  
856 10.1007/b11766995

857 Carlin, B.P. & Louis, T.A., (2000). *Bayes and empirical Bayes methods for data analysis*,  
858 Chapman & Hall, London.

859 Choy, G.L. & Boatwright, J.L., 1995. Global patterns of radiated seismic energy and  
860 apparent stress, *J. Geophys. Res.: Solid Earth*, **100**, B9, 18,205-18,228.

861 CPTI Working Group, 2004. Catalogo Parametrico dei Terremoti Italiani, version 2004  
862 (CPTI04), INGV, Bologna, available on <http://emidius.mi.ingv.it/CPTI04/>

863 DISS Working Group, 2007. Database of Individual Seismogenic Sources (DISS), Version  
864 3.0.2: A compilation of potential sources for earthquakes larger than M 5.5 in Italy and  
865 surrounding areas, <http://diss.rm.ingv.it/diss/>, © INGV 2007 - Istituto Nazionale di  
866 Geofisica e Vulcanologia, Rome , Italy, DOI:10.6092/INGV.IT-DISS3.0.2

867 Gilks, W.R., Richardson, S. & Spiegelhalter, D.J., eds., 1996. *Markov chain Monte Carlo*  
868 *in Practice*, Chapman & Hall, London.

869 Gneiting, T. & Raftery, A.E., 2007. Strictly proper scoring rules, prediction, and estima-  
870 tion, *J. Am. Stat. Assoc.*, **102**, 359-378.

- 871 Hawkes, A.G. & Oakes, D.A., 1974. A cluster process representation of a self-exciting  
872 process, *J. Appl. Probab.*, 11, 493-503.
- 873 Herrmann, R., Malagnini, L. & Munafo, I., 2011. Regional moment tensors of  
874 the 2009 L'Aquila earthquake sequence, *Bull. Seism. Soc. Am.*, 101, 975-993,  
875 doi:10.1785/0120100184.
- 876 International Mathematics and Statistics Library (IMSL) Numerical Libraries, Version  
877 4.0, 2000. Rogue Wave Software, Inc.
- 878 Isham, V. & Westcott, M., 1979. A self-correcting point process, *Stochastic Processes and*  
879 *Their Applications*, 8, 335-347.
- 880 Italian Seismological Instrumental and parametric Data-basE, 2010. *Italian Seismic*  
881 *Bulletin*, Istituto Nazionale di Geofisica e Vulcanologia, Roma, Italy, available on  
882 <http://iside.rm.ingv.it>. Last accessed date June 3, 2015.
- 883 Jiang, M., Zhou, S., Chen, Y.J. & Ai, Y., 2011. A new multidimensional stress release  
884 statistical model based on coseismic stress transfer, *Geophys. J. Int.*, 187, 3, 1479-1494.
- 885 Kagan, Y.Y., 1991. Likelihood analysis of earthquake catalogue, *Geophys. J. Int.*, 106,  
886 135-148.
- 887 Kanamori, H., 1977. The energy release in great earthquakes, *J. Geophys. Res.: Solid*  
888 *Earth*, 82, 2981-2987.
- 889 Kanamori, H. & Brodsky, E.E., 2004. The physics of earthquakes, *Reports on Progress in*  
890 *Physics*, 67, 1429-1496.
- 891 Kanamori, H. & Heaton, T.K., 2000. Microscopic and macroscopic physics of earthquakes,  
892 *Geocomplexity and the Physics of Earthquakes*, Geophysical Monograph 20, AGU, 127-  
893 141.
- 894 Kanamori, H., Mori, J., Hauksson, E., Heaton, T.H., Hutton, L.K. & Jones, L.M., 1993.  
895 Determination of earthquake energy release and  $M_L$  using terrascope, *Bull. Seism. Soc.*  
896 *Am.*, 83, 330-346.

- 897 Kass, R.E. & Raftery, A.E., 1995. Bayes factor, *J. Am. Stat. Ass.*, **90**, 430, 773-795.
- 898 Kuehn, N.M., Hainzl, S. & Scherbaum, F., 2008. Non-Poisson earthquake occurrence in  
899 coupled stress release models and its effect on seismic hazard, *Geophys. J. Int.*, **174**,  
900 649-658.
- 901 Lenart, A., 2014. The moments of Gompertz distribution and maximum like-  
902 lihood estimation of its parameters, *Scand. Actuar. J.*, 2014:3, 255-277,  
903 doi:10.1080/03461238.2012.687697
- 904 Maercklin, N., Zollo, A., Orefice, A., Festa, G., Emolo, A., De Matteis, R., Delouis, B. &  
905 Bobbio, A., 2011. The effectiveness of a distant accelerometer array to compute seismic  
906 source parameters: The April 2009 L'Aquila earthquake case history, *Bull. Seism. Soc.*  
907 *Am.*, 101, 354-365, doi:10.1785/0120100124.
- 908 Matsu'ura, R.S., 1986. Precursory quiescence and recovery of aftershock activities before  
909 some large aftershocks. *Bulletin of the Earthquake Research Institute*, University of  
910 Tokyo, 61, 1-65.
- 911 Meletti, C., Galadini, F., Valensise, G., Stucchi, M., Basili, R., Barba, S., Vannucci, G.  
912 & Boschi, E., 2008. A seismic source zone model for the seismic hazard assessment of  
913 the Italian territory, *Tectonophysics*, **450**, 85-108, doi.10.1016/j.tecto.2008.01.003.
- 914 MPS Working Group 2004, 2004. Redazione della mappa di Pericolosità Sismica Pre-  
915 vista dall'Ordinanza PCM 3274 del 20 Marzo 2003. *Rapporto Conclusivo per il Diparti-*  
916 *mento della Protezione Civile*, Milano-Roma, INGV, 2004 April. 65 pps., 5 appendixes;  
917 <http://zonesismiche.mi.ingv.it>.
- 918 Ogata, Y., 1988. Statistical models for earthquake occurrences and residual analysis for  
919 point processes, *J. Amer. Statist. Assoc.*, **83**, 401, 9-27.
- 920 Ogata, Y., 1997. Detection of precursory relative quiescence before great earthquakes  
921 through a statistical model, *J. Geophys. Res.: Solid Earth*, 97, 19, 845-19,871.

- 922 Ogata, Y., 1999. Seismicity analysis through point-process modeling: a review, In *Seis-*  
923 *micity Patterns, Their Statistical Significance and Physical Meaning* (eds. Wyss, M.,  
924 Shimazaki, K. & Ito, A.) (Birkhäuser, Basel), *Pure Appl. Geophys.*, 155, 471–507.
- 925 Pondrelli, S., Salimbeni, S., Morelli, A., Ekström, G., Olivieri, M. & Boschi, E., 2010. Seis-  
926 mic moment tensors of the April 2009, L’Aquila (Central Italy) earthquake sequence,  
927 *Geophys. J. Int.*, **180**, 238-242, doi: 10.1111/j.1365-246X.2009.04418.x
- 928 R Development Core Team, 2006. *R: A Language and Environment for Statistical Com-*  
929 *puting*, R Foundation for Statistical computing, Vienna, Austria, ISBN 3-900051-07-0,  
930 URL [www.r-project.org](http://www.r-project.org)
- 931 Reid, H.F., 1910. *The Mechanics of the Earthquake. The California Earthquake of April*  
932 *18, 1906*, Report of the State Investigation Commission, Vol. 2, Carnegie Institution of  
933 Washington, Washington, D.C.
- 934 Rotondi, R. & Garavaglia, E., 2002. Statistical analysis of the completeness of a seismic  
935 catalogue, *Natural Hazards*, 25, 3, 245-258.
- 936 Rotondi, R. & Varini, E., 2007. Bayesian inference of stress release models applied to  
937 some Italian seismogenic zones, *Geophys. J. Int.*, **169**, 1, 301-314.
- 938 Rovida, A., Camassi, R., Gasperini, P. & Stucchi, M., eds., 2011. CPTI11, the  
939 2011 version of the Parametric Catalogue of Italian Earthquakes. Milano, Bologna,  
940 <http://emidius.mi.ingv.it/CPTI>
- 941 Scognamiglio, L., Tinti, E., Michelini, A., Dreger, D.S., Cirella, A., Cocco, M., Mazza,  
942 S. & Piatanesi, A., 2010. Fast determination of moment tensors and rupture history:  
943 What has been learned from the 6 April 2009 L’Aquila earthquake sequence, *Bull.*  
944 *Seism. Soc. Am.*, 81, 892-906, doi:10.1785/gssrl.81.6.892.
- 945 Senatorski, P., 2005. A macroscopic approach towards earthquake physics: the meaning  
946 of the apparent stress, *Physica A*, 358, 551-574.

- 947 Senatorski, P., 2006. Fluctuations, trends and scaling of the energy radiated by heteroge-  
948 neous seismic sources, *Geophys. J. Int.*, **166**, 267-276.
- 949 Senatorski, P., 2007. Apparent stress scaling and statistical trends, *Phys. Earth Planet.*  
950 *Inter.*, **160**, 230-244.
- 951 Smith, B.J., 2000. Bayesian Output Analysis Program - (BOA) Version 1.1 User's Manual,  
952 Department of Biostatistics, School of Public Health, University of Iowa.
- 953 Smith, B.J., 2007. boa: An R package for MCMC output convergence assessment  
954 and Posterior inference, *Journal of Statistical Software*, **21**, 11, 37 pp., available on  
955 <http://www.jstatsoft.org/>
- 956 Stucchi, M., Albini, P., Mirto, C. & Rebez, A., 2004. Assessing the completeness of Italian  
957 historical earthquake data, *Annals of Geophysics*, **47**, 2/3, 659-673.
- 958 Varini, E. & Rotondi, R., 2015. Probability distribution of the waiting time in the stress  
959 release model: the Gompertz distribution, *Environmental and Ecological Statistics*, **22**,  
960 3, 493-511, doi:10.1007/s10651-014-0307-2
- 961 Vere-Jones, D., 1978. Earthquake prediction - A statistician's view, *J. Physics Earth*, **26**,  
962 129-146.
- 963 Vere-Jones, D. & Yonglu, D., 1988. A point process analysis of historical earthquakes  
964 from North China, *Earthquake Research in China*, **2**, 2, 165-181.
- 965 Vehtari, A. & Ojanen, J., 2012. A survey of Bayesian predictive methods for model as-  
966 sessment, selection and comparison, *Stat. Surv.*, **6**, 142-228.
- 967 Votsi, I., Tsaklidis, G.M. & Papadimitriou, E.E., 2011. Seismic hazard assessment in  
968 central Ionian Islands area (Greece) based on stress release models, *Acta Geophysica*,  
969 **59**, 4,701-727.
- 970 Wang, A., Vere-Jones, D. & Zheng, X., 1991. Simulation and estimation procedures for  
971 stress release models, in *Stochastic Processes and Their Applications, Lecture Notes in*

- 972 *Econometrics and Mathematical Systems*, Vol. 370, pp. 11-27, eds. Beckmann, M.J.,  
973 Gopalan, M.N. & Subramanian, R., Springer, Berlin.
- 974 Watanabe, S., 2010. Asymptotic equivalence of Bayes cross validation and widely ap-  
975 plicable information criterion in singular learning theory, *J. Mach. Learn. Res.*, **11**,  
976 3571-3594.
- 977 Wells, D.L. & Coppersmith, K.L., 1994. New relationships among magnitude, rupture  
978 length, rupture width, rupture area, and surface displacement, *Bull. Seism. Soc. Am.*,  
979 **84**, 4, 974-1002.
- 980 Zheng, X. & Vere-Jones, D., 1991. Application of stress release models to historical earth-  
981 quakes from North China, *Pure Appl. Geophys.*, **135**, 4, 559-576.
- 982 Zheng, X. & Vere-Jones, D., 1994. Further applications of the stochastic stress release  
983 model to historical data, *Tectonophysics*, 229, 101-121.



## A Completeness of the catalog: statistical analysis

Let us consider a catalog that covers the time interval  $(T_0, T_f)$ , and suppose that there is a point  $s$  in this interval in which the seismicity rate changes, so that the global model for the number of events within the given time interval is the mixture of two Poisson processes, with the intensity function  $\lambda(t)$  given by:

$$\lambda(t) = h_1 I_{t < s}(t) + h_2 I_{t \geq s}(t) \quad (33)$$

where  $h_1$  and  $h_2$  are the seismicity rate of the pre-complete and complete parts, respectively. According to the Bayesian approach, both the rates and the position of the changepoint  $s$  are random variables; we assume that both  $h_1$  and  $h_2$  follow the prior distribution  $Gamma(a_0, b)$ , with density function  $b^{-a_0} e^{-h/b} h^{a_0-1} / \Gamma(a_0)$ , while  $s$  is uniformly distributed on  $(T_0, T_f)$ . *A priori* information on the variability of the yearly occurrence rate is inferred from the general considerations of the average number of events under examination. In the present study, we considered the shocks with  $M_w \geq 5.3$  recorded in the CPTI04 for 1600-2002, a period generally considered sufficiently complete in the literature on Italian seismicity (Stucchi et al. , 2004). The uncertainty on the occurrence rate is then incorporated in the model through a further hierarchical level by considering  $b$  as an *InvGamma*( $c_0, f_0$ ) distributed random variable. In our case, parameter  $a_0$  and hyperparameters  $c_0$  and  $f_0$  are set as  $a_0 = 0.1$ ,  $c_0 = 3$ , and  $f_0 = 5$ . For the time interval  $(T_0, T_f)$ , we set  $T_f = 2003$ , as the end of the CPTI04, while  $T_0$  varies in each MR. To balance the final gap between  $T_f$  and the time  $t_n$  of the last event, we approximately set  $T_0$  back by  $(T_f - t_n)$ , so we have  $T_0 = t_1 - T_f + t_n$ , with  $t_1$  as the time of the first event in the dataset.

We estimate the model parameters  $h_1$ ,  $h_2$ ,  $s$ , and  $b$  through Gibbs sampling, one of the most popular MCMC methods, which is a class of methods that are based on the simulation of samples of dependent values that constitute a realization of a stationary Markov chain asymptotically convergent in distribution to the quantity to estimate (Gilks et al. , 1996). For a detailed description of the algorithm, see Rotondi & Garavaglia (2002).

1011 Model estimations provide the posterior probability distributions of the parameters; the  
 1012 most probable value (mode) of  $s$  is assumed as the beginning of the complete part of  
 1013 the dataset, whereas the posterior mean of  $h_2$  gives the estimate of the corresponding  
 1014 seismicity rate. We recall that measures of the uncertainty of the estimates, expressed  
 1015 through measures of location (mean, mode) and dispersion (variance, quantiles) can be  
 1016 drawn from the posterior distribution of the parameters.

## 1017 B McMC methods

1018 We implemented the Metropolis-Hastings algorithm to generate a Markov chain for each  
 1019 parameter, as summarized below. Assuming some transition kernel  $q(\theta, \theta^*)$  (called the  
 1020 *proposal distribution*), from which it is easy to simulate, such that:

- 1021 1. Initialize the chain by simulating  $\theta^{(0)}$  from the prior distribution  $\pi_0(\theta)$ , and set the  
 1022 iteration counter  $j = 1$ .
- 1023 2. Generate a *proposed* value  $\theta^*$  using the kernel  $q(\theta^{(j-1)}, \theta^*)$ .
- 1024 3. Evaluate the *acceptance probability*  $\alpha(\theta^{(j-1)}, \theta^*)$  of the proposed move, where:  
 1025 
$$\alpha(\theta^{(j-1)}, \theta^*) = \min \left\{ 1, \frac{\pi(\theta^* | data) q(\theta^*, \theta^{(j-1)})}{\pi(\theta^{(j-1)} | data) q(\theta^{(j-1)}, \theta^*)} \right\} .$$
- 1026 4. Put  $\theta^{(j)} = \theta^*$  with probability  $\alpha(\theta^{(j-1)}, \theta^*)$ , otherwise retain the current value of  $\theta$ :  
 1027  $\theta^{(j)} = \theta^{(j-1)}$ .
- 1028 5. Change the counter from  $j$  to  $j + 1$  and return to step 2.

1029 Given a function  $g(\theta)$ , under suitable regularity conditions it has been shown that the  
 1030 ergodic mean  $\frac{\sum_{j=1}^R g(\theta^{(j)})}{R}$  converges almost surely to  $E_{\theta|data} \{g(\theta)\}$  as  $R \rightarrow \infty$ ; therefore,  
 1031 if we set  $g(\theta) = \theta$  or  $g(\theta) = [\theta - E(\theta)]^2$ , by applying this theorem, we obtain the estimate  
 1032 of the mean and variance of  $\theta$  respectively. It is important to note that the density  
 1033 of interest  $\pi(\cdot | data)$  only enters in the acceptance probability as a ratio, and so the  
 1034 method can be used when this density is known up to a normalizing constant, for instance

1035  $\pi(\theta \mid data) \propto \mathcal{L}(data \mid \theta) \pi_0(\theta)$ . The Markov chain generated through the algorithm is  
1036 reversible and has a stationary distribution  $\pi(\theta \mid data)$  irrespective of the choice of the  
1037 proposal distribution. The critical point of this method is how to assess the convergence  
1038 of the sampler; to solve this issue, we first discard the 'burn-in' of the simulated sequence  
1039  $\{\theta^{(j)}\}_{j=0}^R$ , i.e., its initial part (ca. 10%-20%), to reduce the dependence on the initial  
1040 value; then we apply one of the software tools that are available for MCMC convergence  
1041 diagnostics. In particular, we choose the open-source package BOA (Smith , 2005) for the  
1042 R system for statistical computing (R Development Core Team , 2006), and check that  
1043 all of the generated sequences do not fail the following tests: Geweke test, Heidelberger  
1044 & Welch test, and Raftery & Lewis test (Smith , 2007). Table B2 reports the prior and  
1045 proposal distributions used in the MCMC algorithm for the parameter estimation: we  
1046 note that the mean of every proposal is given by the current value of the chain, whereas  
1047 the value of the variance is assigned through some pilot runs of the algorithm so that  
1048 the acceptance probability varies in the range of 25% to 40% - a range that has been  
1049 suggested in the statistical literature to be the best. As an example, Figure B2 shows the  
1050 prior density and the kernel density estimates of the posterior density of each parameter  
1051 of the various models obtained by analyzing the data from MR<sub>4</sub>.

	$t$	$\hat{\alpha}$	$\hat{\beta}$	$\hat{\rho}$
MR <sub>3</sub>	(end of the catalog) 2002/12/31	-1.80	1.89E-1	5.20E-2
	(event) 2003/09/14	-1.83	1.90E-1	5.52E-2
	(event) 2008/12/23	-1.83	1.93E-1	5.53E-2
	(event) 2012/05/20	-1.85	1.94E-1	5.68E-2
	2012/12/31	-1.84	1.95E-1	5.62E-2
MR <sub>4</sub>	(end of the catalog) 2002/12/31	-2.13	5.36E-1	3.31E-2
	(event) 2009/04/06	-2.15	5.32E-1	3.35E-2
	2012/12/31	-2.13	5.52E-1	3.29E-2

Table B1: Parameter estimates of the  $\mathbf{R}_S$  models for MR<sub>3</sub> and MR<sub>4</sub>, updated by enlarging the history  $\mathcal{H}_t$  on which the intensity function is conditioned.

Model	Region	Prior distribution			Proposal distribution		
		$\alpha$	$\beta$	$\rho$	$\alpha$	$\beta$	$\rho$
<b>R<sub>B</sub></b>	MR <sub>1</sub>	N(-4.00; 13.0)	$\Gamma(0.50; 2.0E-1)$	$\Gamma(0.10; 8.1E-3)$	N(*; 1.7)	LogN(*; 4.0E-2)	LogN(*; 4.0E-4)
	MR <sub>2</sub>	N(-2.50; 5.0)	$\Gamma(0.10; 8.1E-3)$	$\Gamma(0.20; 3.2E-2)$	N(*; 8.0E-1)	LogN(*; 7.5E-3)	LogN(*; 1.5E-2)
	MR <sub>3</sub>	N(-1.00; 8.0E-1)	$\Gamma(0.05; 2.0E-3)$	$\Gamma(0.40; 1.3E-1)$	N(*; 3.0E-1)	LogN(*; 1.8E-3)	LogN(*; 3.0E-2)
	MR <sub>4</sub>	N(-1.50; 1.8)	$\Gamma(0.05; 2.0E-3)$	$\Gamma(0.40; 1.3E-1)$	N(*; 3.5E-1)	LogN(*; 5.0E-4)	LogN(*; 4.0E-2)
	MR <sub>5</sub>	N(-2.00; 3.2)	$\Gamma(0.20; 3.2E-2)$	$\Gamma(0.40; 1.3E-1)$	N(*; 9.0E-1)	LogN(*; 1.0E-2)	LogN(*; 3.0E-2)
	MR <sub>6</sub>	N(-2.50; 5.0)	$\Gamma(0.10; 8.1E-3)$	$\Gamma(0.50; 2.0E-1)$	N(*; 8.0E-1)	LogN(*; 2.0E-3)	LogN(*; 2.3E-2)
	MR <sub>7</sub>	N(-2.00; 3.2)	$\Gamma(0.02; 3.2E-4)$	$\Gamma(1.00; 8.1E-1)$	N(*; 4.0E-1)	LogN(*; 1.6E-4)	LogN(*; 5.0E-1)
	MR <sub>8</sub>	N(-3.00; 7.0)	$\Gamma(0.03; 7.0E-4)$	$\Gamma(0.20; 3.2E-2)$	N(*; 7.0E-1)	LogN(*; 4.0E-4)	LogN(*; 6.0E-2)
<b>R<sub>M</sub></b>	MR <sub>1</sub>	N(-5.00; 20.2)	$\Gamma(0.50; 2.0E-1)$	$\Gamma(0.30; 7.0E-2)$	N(*; 2.0)	LogN(*; 6.0E-3)	LogN(*; 1.0E-3)
	MR <sub>2</sub>	N(-2.50; 5.0)	$\Gamma(0.03; 7.0E-4)$	$\Gamma(0.80; 5.0E-1)$	N(*; 8.0E-1)	LogN(*; 3.0E-4)	LogN(*; 4.0E-1)
	MR <sub>3</sub>	N(-1.00; 8.0E-1)	$\Gamma(0.02; 3.2E-4)$	$\Gamma(0.80; 5.0E-1)$	N(*; 3.0E-1)	LogN(*; 2.0E-4)	LogN(*; 2.5E-1)
	MR <sub>4</sub>	N(-1.50; 1.8)	$\Gamma(0.003; 7.0E-6)$	$\Gamma(3.00; 7.0)$	N(*; 3.0E-1)	LogN(*; 3.0E-6)	LogN(*; 5.0)
	MR <sub>5</sub>	N(-2.00; 3.2)	$\Gamma(0.01; 8.1E-5)$	$\Gamma(2.00; 3.2)$	N(*; 9.0E-1)	LogN(*; 5.0E-5)	LogN(*; 3.5)
	MR <sub>6</sub>	N(-2.50; 5.0)	$\Gamma(0.01; 8.1E-5)$	$\Gamma(6.00; 30.0)$	N(*; 8.0E-1)	LogN(*; 1.5E-5)	LogN(*; 2.4)
	MR <sub>7</sub>	N(-2.00; 3.2)	$\Gamma(0.001; 1.0E-6)$	$\Gamma(12.0; 1.1E+2)$	N(*; 4.0E-1)	LogN(*; 4.0E-7)	LogN(*; 1.0E+2)
	MR <sub>8</sub>	N(-3.00; 7.0)	$\Gamma(0.001; 1.0E-6)$	$\Gamma(8.00; 5.0E+1)$	N(*; 7.0E-1)	LogN(*; 3.0E-7)	LogN(*; 8.0E+1)
<b>R<sub>E</sub></b>	MR <sub>1</sub>	N(-5.00; 20.2)	$\Gamma(1.50; 1.8)$	$\Gamma(0.05; 2.0E-3)$	N(*; 2.0)	LogN(*; 8.0E-2)	LogN(*; 1.0E-4)
	MR <sub>2</sub>	N(-2.50; 5.0)	$\Gamma(0.04; 1.3E-3)$	$\Gamma(0.30; 7.0E-2)$	N(*; 8.0E-1)	LogN(*; 8.0E-4)	LogN(*; 8.0E-2)
	MR <sub>3</sub>	N(-1.00; 8.0E-1)	$\Gamma(0.04; 1.3E-3)$	$\Gamma(0.30; 7.0E-2)$	N(*; 3.0E-1)	LogN(*; 1.0E-3)	LogN(*; 4.0E-2)
	MR <sub>4</sub>	N(-1.50; 1.8)	$\Gamma(0.004; 1.3E-5)$	$\Gamma(2.00; 3.2)$	N(*; 3.0E-1)	LogN(*; 8.0E-6)	LogN(*; 3.0)
	MR <sub>5</sub>	N(-2.00; 3.2)	$\Gamma(0.02; 3.0E-4)$	$\Gamma(1.00; 8.1E-1)$	N(*; 9.0E-1)	LogN(*; 1.5E-4)	LogN(*; 9.0E-1)
	MR <sub>6</sub>	N(-2.50; 5.0)	$\Gamma(0.02; 3.2E-4)$	$\Gamma(3.00; 7.0)$	N(*; 8.0E-1)	LogN(*; 5.0E-5)	LogN(*; 8.0E-1)
	MR <sub>7</sub>	N(-2.00; 3.2)	$\Gamma(0.001; 1.0E-6)$	$\Gamma(8.00; 5.0E+1)$	N(*; 4.0E-1)	LogN(*; 1.0E-6)	LogN(*; 4.8E+1)
	MR <sub>8</sub>	N(-3.00; 7.0)	$\Gamma(0.001; 1.0E-6)$	$\Gamma(8.00; 5.0E+1)$	N(*; 7.0E-1)	LogN(*; 3.0E-7)	LogN(*; 6.0E+1)
<b>R<sub>S</sub></b>	MR <sub>1</sub>	N(-3.50; 1.0E+1)	$\Gamma(3.00; 7.0)$	$\Gamma(0.01; 8.1E-5)$	N(*; 1.7)	LogN(*; 1.7)	LogN(*; 2.0E-5)
	MR <sub>2</sub>	N(-2.50; 5.0)	$\Gamma(2.00; 3.2)$	$\Gamma(0.04; 1.3E-3)$	N(*; 8.0E-1)	LogN(*; 1.5)	LogN(*; 8.0E-5)
	MR <sub>3</sub>	N(-1.00; 8.1E-1)	$\Gamma(0.30; 7.0E-2)$	$\Gamma(0.08; 5.0E-3)$	N(*; 3.0E-1)	LogN(*; 6.0E-2)	LogN(*; 1.0E-3)
	MR <sub>4</sub>	N(-1.50; 1.8)	$\Gamma(1.00; 8.1E-1)$	$\Gamma(0.04; 1.3E-3)$	N(*; 3.0E-1)	LogN(*; 3.8E-1)	LogN(*; 8.0E-5)
	MR <sub>5</sub>	N(-2.00; 3.2)	$\Gamma(3.00; 7.0)$	$\Gamma(0.04; 1.3E-3)$	N(*; 9.0E-1)	LogN(*; 4.0)	LogN(*; 6.0E-5)
	MR <sub>6</sub>	N(-2.50; 5.0)	$\Gamma(2.00; 3.2)$	$\Gamma(0.03; 7.0E-4)$	N(*; 8.0E-1)	LogN(*; 1.2)	LogN(*; 3.0E-5)
	MR <sub>7</sub>	N(-2.00; 3.2)	$\Gamma(0.40; 1.3E-1)$	$\Gamma(0.08; 5.0E-3)$	N(*; 4.0E-1)	LogN(*; 7.0E-2)	LogN(*; 1.0E-3)
	MR <sub>8</sub>	N(-3.00; 7.0)	$\Gamma(1.50; 1.8)$	$\Gamma(0.01; 8.1E-5)$	N(*; 7.0E-1)	LogN(*; 5.0E-1)	LogN(*; 3.0E-5)

Table B2: Prior and proposal distributions of the model parameters  $\theta = (\alpha, \beta, \rho)$  adopted in the McMC estimation method. The mean and variance of every prior/ proposal distribution are reported, so that, e.g., for the Gamma distribution, the shape and scale parameters can be derived. The mean of each proposal distribution is set equal to the current value of the corresponding parameter in the Markov chain.

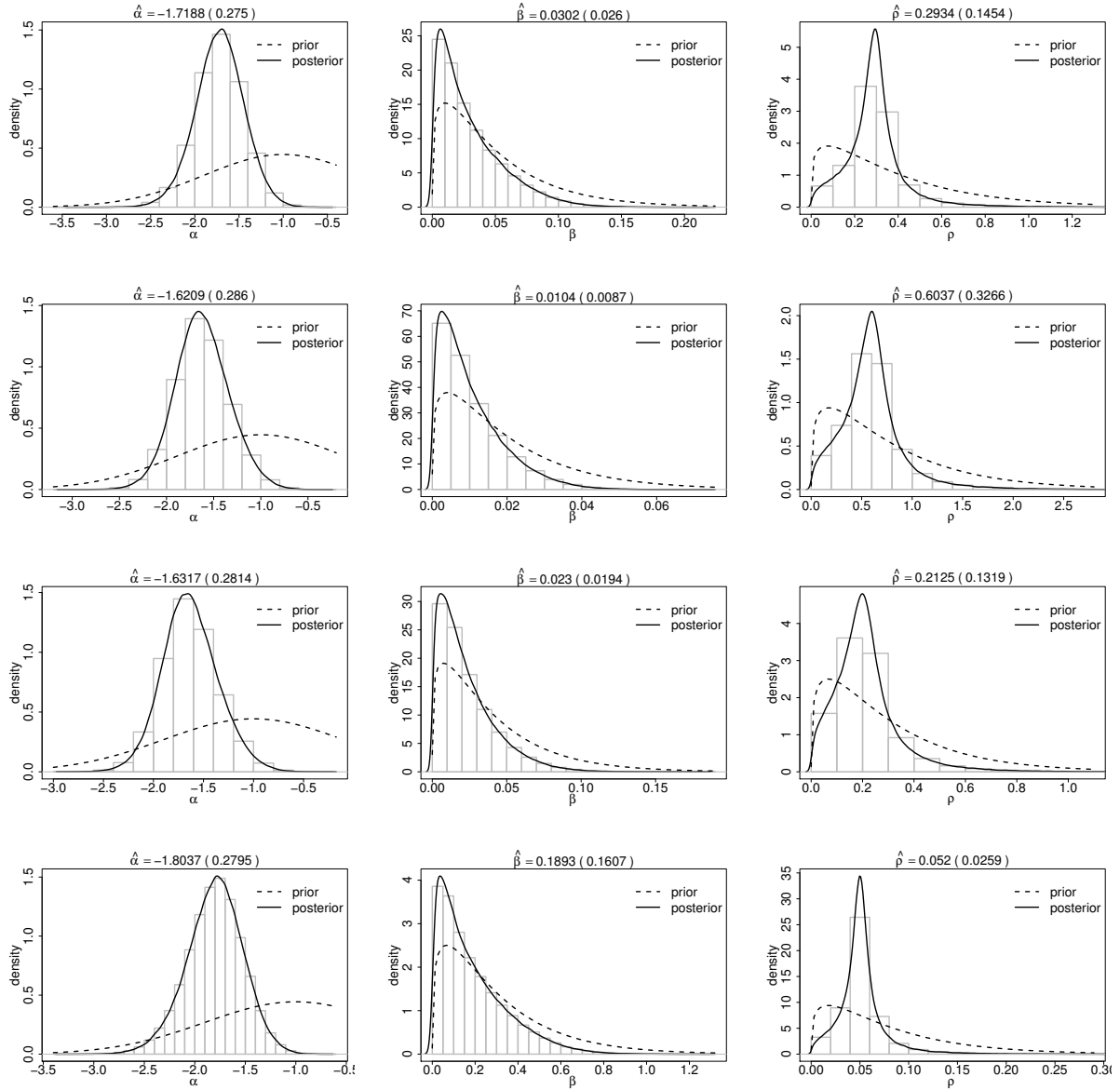


Figure B1: From top to bottom, the  $\mathbf{R}_B$ ,  $\mathbf{R}_M$ ,  $\mathbf{R}_E$ , and  $\mathbf{R}_S$  models. Prior density functions (dotted line); histograms and kernel posterior density estimates (solid line) computed from the values of the Markov chain of each parameter  $\alpha$ ,  $\beta$ , and  $\rho$ . Example taken from  $\text{MR}_3$ .

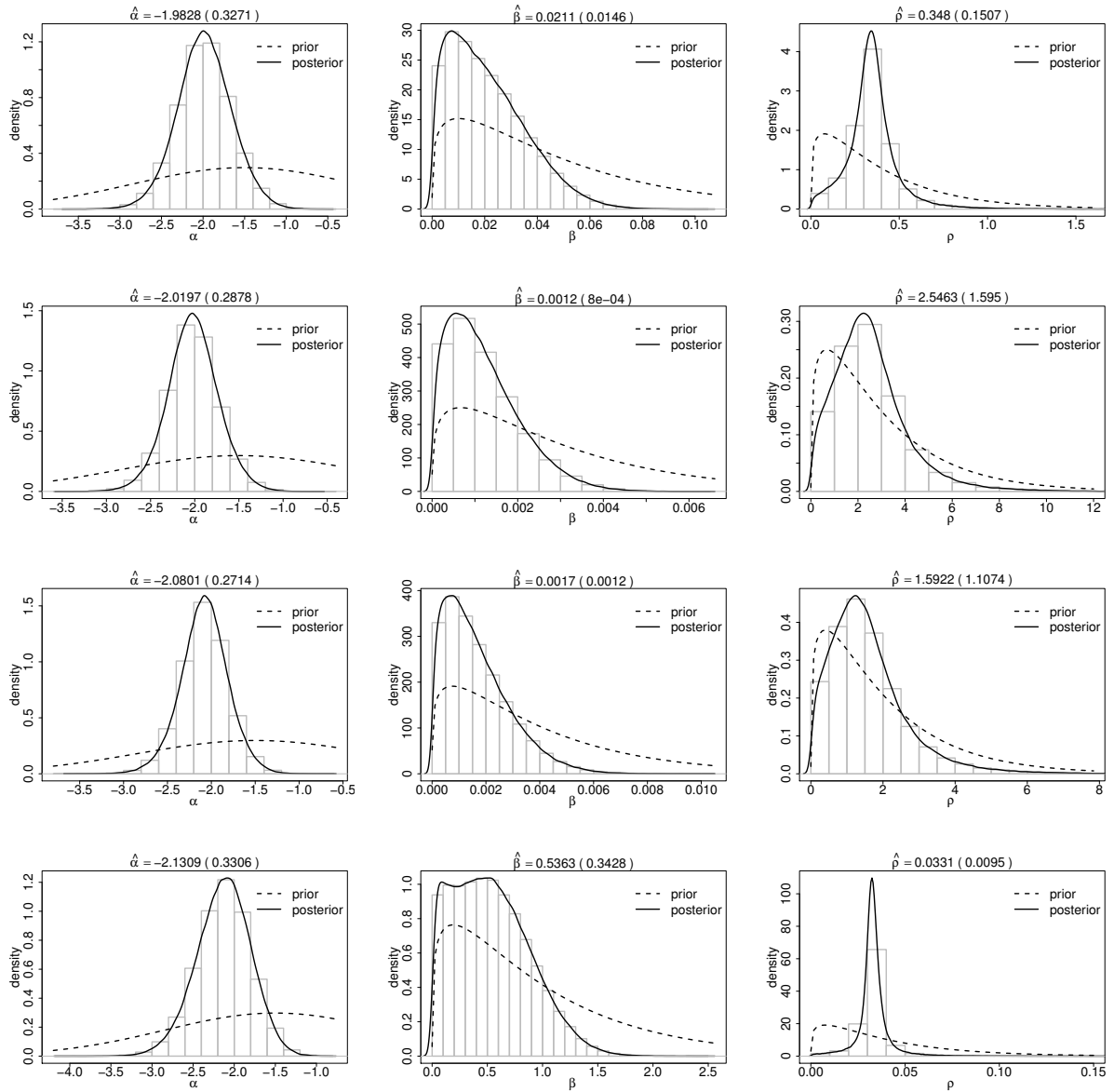


Figure B2: Same as Figure B1. Example taken from MR<sub>4</sub>.

## C Retrospective validation

1053 Figures C1-C7 summarize the retrospective analyses of the forecasts issued at the occur-  
 1054 rence time of every event in the datasets.

Region	Model	HPD 75%	HPD 90%	Median	Mean (st.dev.)
MR <sub>1</sub>	$R_B$	2003.0-2061.6	2003.0-2106.3	2031.4	2048.3 (41.4)
	$R_M$	2003.0-2139.8	2003.0-2201.6	2085.0	2101.2 (39.7)
	$R_E$	2003.0-2304.0	2003.0-2359.0	2191.6	2204.2 (48.9)
	$R_S$	2003.0-2066.5	2003.0-2119.2	2032.7	2053.1 (51.2)
MR <sub>2</sub>	$R_B$	2003.0-2026.8	2003.0-2043.2	2014.8	2020.5 (16.7)
	$R_M$	2003.0-2028.4	2003.0-2047.1	2015.3	2022.0 (18.9)
	$R_E$	2003.0-2027.7	2003.0-2046.0	2014.9	2021.5 (18.9)
	$R_S$	2003.0-2024.0	2003.0-2036.9	2013.8	2018.1 (13.4)
MR <sub>3</sub>	$R_B$	2003.0-2010.8	2003.0-2016.2	2006.8	2008.7 ( 5.7)
	$R_M$	2003.0-2010.5	2003.0-2015.8	2006.7	2008.5 ( 5.6)
	$R_E$	2003.0-2010.5	2003.0-2015.8	2006.7	2008.5 ( 5.6)
	$R_S$	2003.0-2011.1	2003.0-2016.7	2007.0	2008.9 ( 5.9)
MR <sub>4</sub>	$R_B$	2003.0-2015.5	2003.0-2024.1	2009.2	2012.1 ( 9.0)
	$R_M$	2003.0-2015.0	2003.0-2023.5	2008.9	2011.8 ( 9.0)
	$R_E$	2003.0-2014.7	2003.0-2022.9	2008.8	2011.6 ( 8.8)
	$R_S$	2003.0-2015.6	2003.0-2023.5	2009.4	2012.0 ( 8.3)
MR <sub>5</sub>	$R_B$	2003.0-2021.0	2003.0-2034.1	2011.8	2016.5 (13.5)
	$R_M$	2003.0-2020.9	2003.0-2034.1	2011.6	2016.3 (13.8)
	$R_E$	2003.0-2020.8	2003.0-2033.9	2011.6	2016.3 (13.7)
	$R_S$	2003.0-2019.3	2003.0-2029.6	2011.6	2015.2 (11.1)
MR <sub>6</sub>	$R_B$	2003.0-2033.8	2003.0-2054.5	2018.6	2025.8 (21.6)
	$R_M$	2003.0-2037.1	2003.0-2059.6	2020.2	2028.0 (23.5)
	$R_E$	2003.0-2039.3	2003.0-2062.8	2021.4	2029.5 (24.4)
	$R_S$	2003.0-2031.7	2003.0-2049.6	2018.0	2024.1 (19.2)
MR <sub>7</sub>	$R_B$	2003.0-2014.5	2003.0-2022.7	2008.6	2011.5 ( 8.7)
	$R_M$	2003.0-2015.1	2003.0-2023.7	2009.0	2011.9 ( 9.1)
	$R_E$	2003.0-2015.4	2003.0-2024.1	2009.1	2012.1 ( 9.3)
	$R_S$	2003.0-2014.0	2003.0-2021.9	2008.4	2011.1 ( 8.3)
MR <sub>8</sub>	$R_B$	2003.0-2025.7	2003.0-2042.5	2014.0	2019.9 (17.5)
	$R_M$	2003.0-2023.1	2003.0-2038.2	2012.7	2018.0 (15.7)
	$R_E$	2003.0-2022.9	2003.0-2037.7	2012.6	2017.8 (15.5)
	$R_S$	2003.0-2035.3	2003.0-2054.0	2019.7	2025.7 (19.5)

Table C1: Prospective forecast after the end date of the learning catalog. Summary of the estimated probability distributions of the times to next event in each MR provided by all of the models: 75% and 90% HPD intervals, median, mean, and standard deviation.

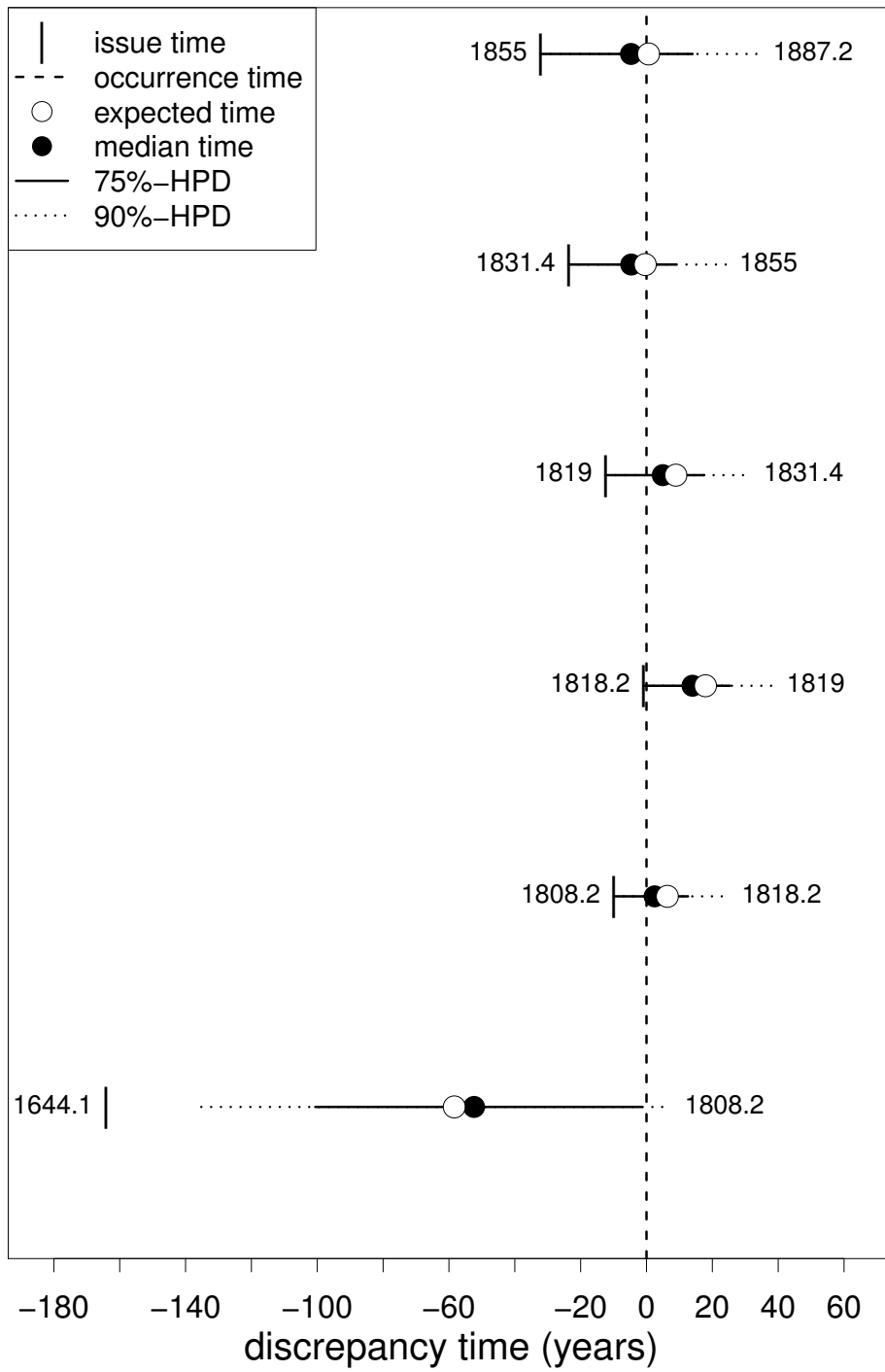


Figure C1: As for Figure 8, validation results related to macroregion MR<sub>1</sub> -  $\mathbf{R}_E$  model.



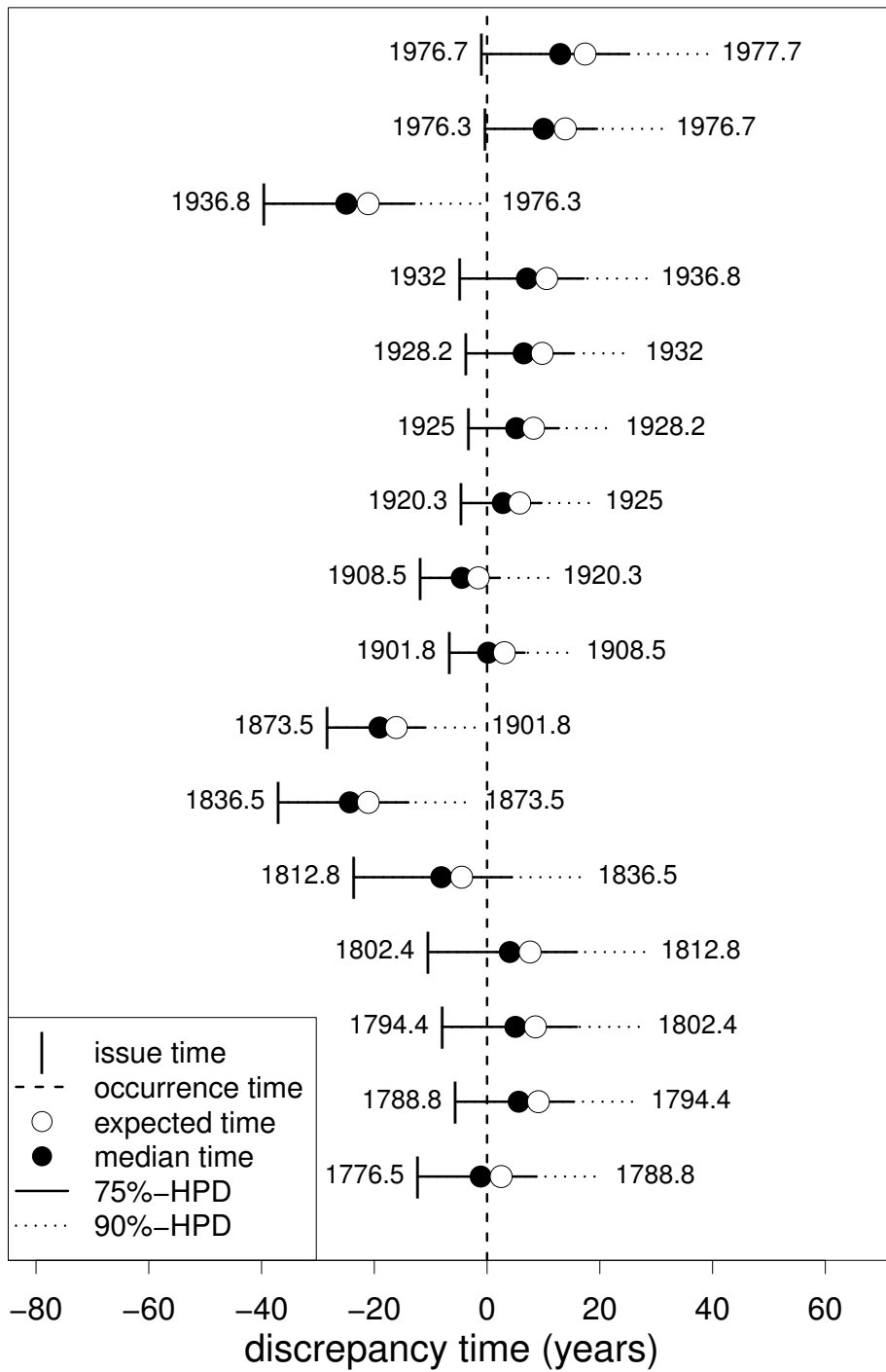


Figure C2: As for Figure 8, validation results related to macroregion MR<sub>2</sub> - **R<sub>S</sub>** model.

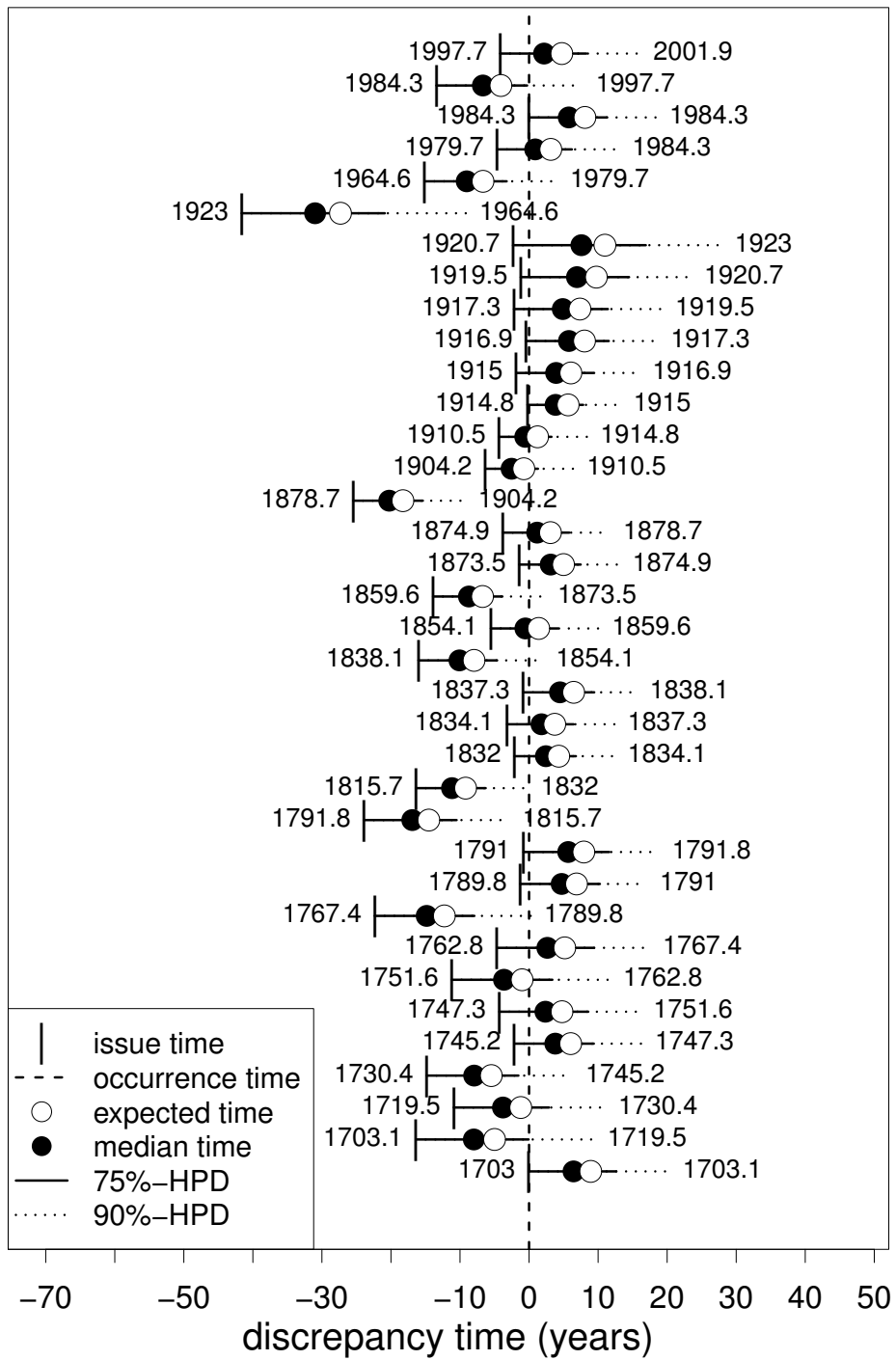


Figure C3: As for Figure 8, validation results related to macroregion MR<sub>4</sub> - **R<sub>S</sub>** model.

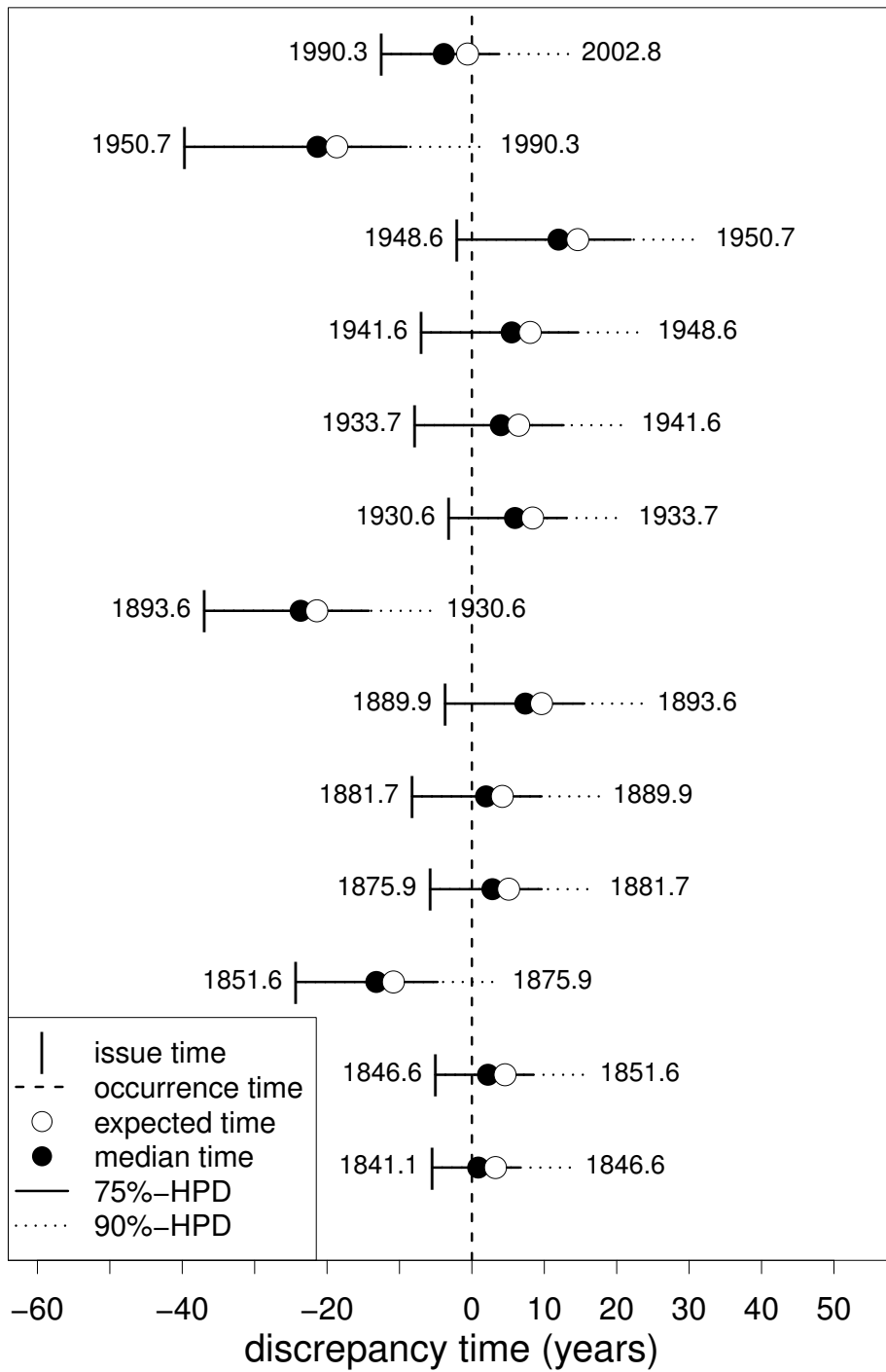


Figure C4: As for Figure 8, validation results related to macroregion MR<sub>5</sub> - **R<sub>S</sub>** model.

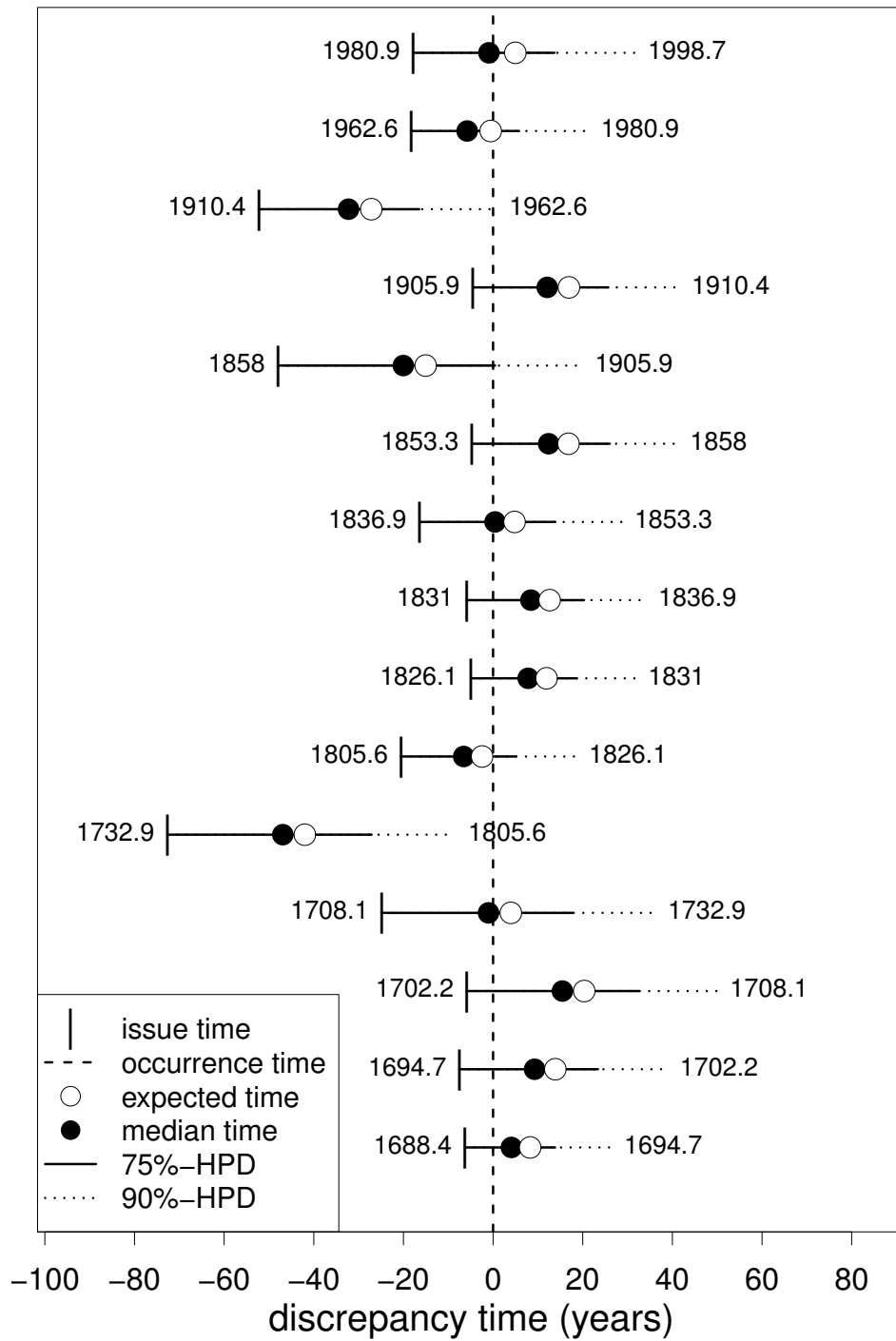


Figure C5: As for Figure 8, validation results related to macroregion MR<sub>6</sub> -  $\mathbf{R}_S$  model.

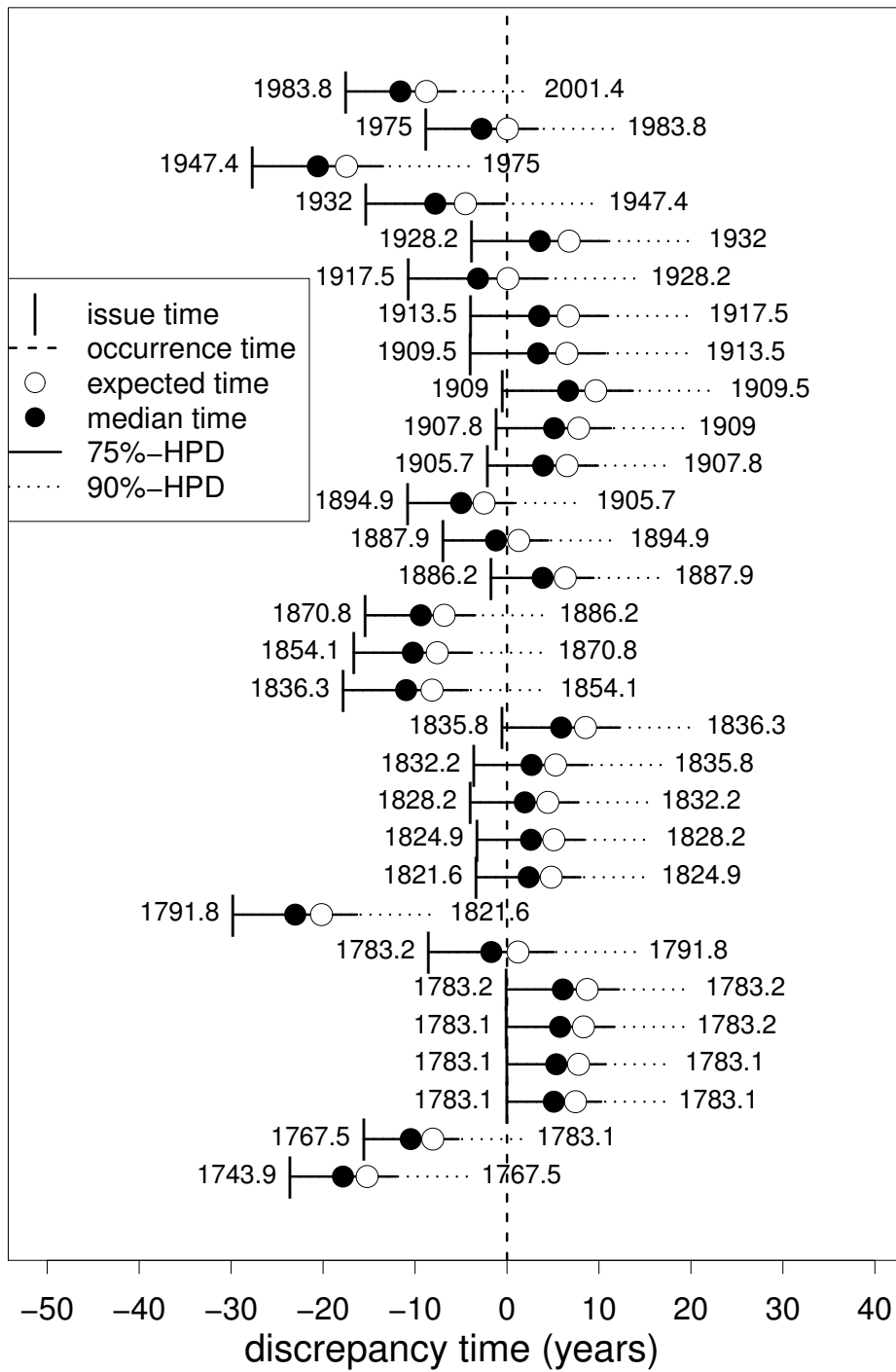


Figure C6: As for Figure 8, validation results related to macroregion MR<sub>7</sub> - **R<sub>S</sub>** model.

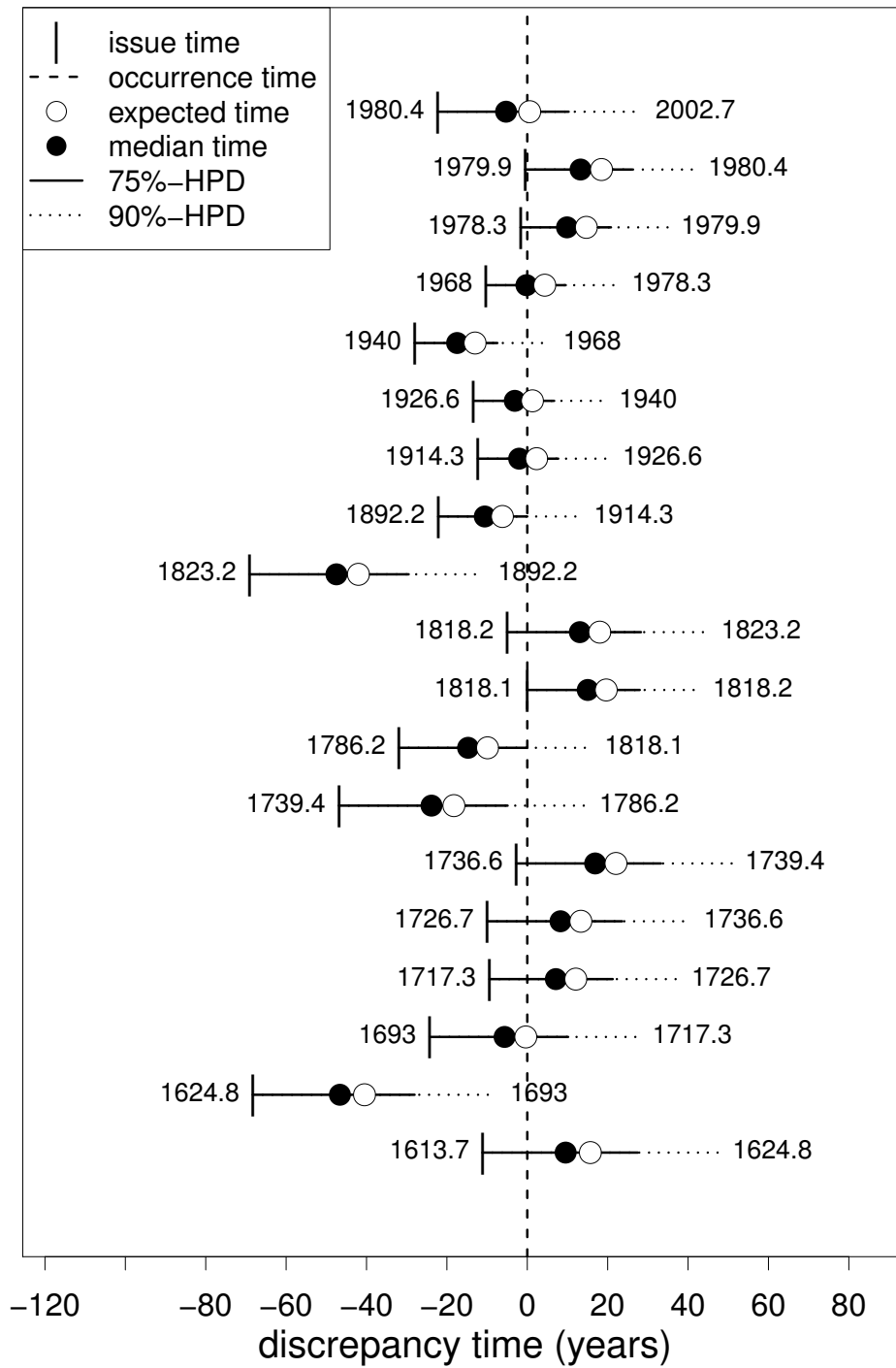


Figure C7: As for Figure 8, validation results related to macroregion MR<sub>8</sub> - **R<sub>S</sub>** model.